Title

High-Performance Cannabinoid Sensor Empowered by Plant Hormone Receptors and Antifouling Magnetic Nanorods.

Authors

Li, Zongbo
Shen, Yuyang
Beltrán, Jesús
et al.

Publication Date

2023-09-01

DOI

10.1021/acssensors.3c01488

A High-Performance Cannabinoid Sensor Empowered by Plant Hormone Receptors and Antifouling Magnetic Nanorods

Zongbo Li,[1] Yuyang Shen,[2] Jesús Beltrán,[3,4] Hao Tian[3,4], Matthew Bedewitz[6], Ian Wheeldon,[4,5] Timothy A. Whitehead,[6] Sean R. Cutler[3, 4] and Wenwan Zhong[1, 2, *]

[1]Department of Chemistry; [2]Environmental Toxicology Graduate Program; [3]Department of Botany and Plant Sciences; [4]Institute for Integrative Genome Biology; [5]Department of Chemical and Environmental Engineering, University of California-Riverside, Riverside, CA 92521, U.S.A.

[6]Department of Chemical and Biological Engineering, University of Colorado Boulder, Boulder, CO, USA.

* Corresponding author

Wenwan Zhong, email: wenwan.zhong@ucr.edu

KEYWORDS: cannabinoids; plant hormone sensors; protein receptors; superparamagnetic nanorods; zwitterionic polymer; ELISA-like assay

Abstract

The misuse of cannabinoids and their synthetic variants pose significant threats to public health, necessitating the development of advanced techniques for detection of these compounds in biological or environmental samples. Existing methods face the challenges like lengthy sample pretreatment and laborious antifouling steps. Herein, we present a novel sensing platform using magnetic nanorods coated with zwitterionic polymers for simple, rapid, and sensitive detection of cannabinoids in biofluids. Our technique utilizes the engineered derivatives of the plant hormone receptor *Pyrabactin Resistance 1* (PYR1) as drug recognition elements, and employs the chemical-induced dimerization (CID) mechanism for signal development. Additionally, the magnetic nanorods facilitate efficient target capture and reduce assay duration. Moreover, the zwitterionic polymer coating exhibits excellent antifouling capability, preserving excellent sensor performance in complex biofluids. Our sensors detect cannabinoids in undiluted biofluids like serum, saliva, and urine with a low limit of detection (0.002 pM in saliva, and few pM in urine and serum) and dynamic ranges spanning up to 9 orders of magnitude. Moreover, the PYR1 derivatives demonstrate high specificity, even in the presence of multiple interfering compounds. This work opens new opportunities for sensor development, showcasing the excellent performance of antifouling magnetic nanorods that can be compatible with different recognition units, including receptors and antibodies for detecting a variety of targets.

According to the World Drug Report 2022, cannabis is the most widely used controlled drug worldwide.[1] While cannabinoids found in cannabis, like Δ9 -tetrahydrocannabinol (Δ9-THC) and cannabidiol (CBD), have shown medicinal benefits, including the anti-inflammatory and pain relief properties;[2-3] they also can impair capability of driving, induce negative mental and respiratory health outcomes, and impact the developing brain of adolescents.[4-6] Adding to the concerns is the rising production and use of synthetic cannabinoids (SCs) that can produce strong cannabis-like effects but are marketed as recreational drugs to circumvent legislative control measures.[7] They can induce adverse health effects like seizures, acute respiratory distress syndrome, and multiple organ failure,[8] representing an emerging and ongoing public health and safety threat in the United States.

Timely and proper controls on the abuse of cannabinoids demand the developments of specific and sensitive methods for detection of such drugs in biospecimens. The concentration and form of cannabinoids present in biospecimens upon administration are determined by the drug's pharmacokinetics.[9-10] For example, the concentration of intact Δ9-THC in plasma rapidly decreases after inhalation and can be found at only ~ 1 ng/mL or lower in plasma within 24 hrs.[11-12] Chromatographic separation coupled with multistage mass spectrometry (MS^n) can provide comprehensive analysis and sensitive quantification of the broad spectrum of cannabinoids, achieving limits of detection (LOD) as low as 0.05 ng/mL (~ 0.1 nM of common cannabinoids) in well-equipped labs.[13-14] Quick exposure assessment in clinical and law-enforcement labs at relatively lower costs can be done with Enzyme-Linked Immunosorbent Assays (ELISAs) and related immunoassays, reporting LODs ≥ 1 - 5 ng/mL,[15-16] or Activity-based screening assays that offer LODs in the low ng/mL range.[17-18] Electrochemical sensors are more sensitive and can detect as low as 0.0033 ng/mL (10 pM) Δ9-THC with high feasibility for

field deployment.[9, 19] While these techniques demonstrate good performance, they face two primary challenges: the limited capability to achieve low LOD in unprocessed biological samples without analyte extraction;[13,20-21] and the rapidly emerging SCs that make it difficult to produce the drug recognition units with a matching pace and low cross-reactivity using the conventional ways.[22-24]

To address the need for rapid response to the rapidly emerging cannabinoids, we have developed novel phytocannabinoid diagnostic reagents built from an engineered plant hormone receptor Pyrabactin Resistance 1 (PYR1). The PYR1 recognizes its ligand and through the chemically induced dimerization (CID) mechanism, forming a stable PYR1–ligand–protein phosphatase (PP2C) complex.[25] While the CID inhibits the phosphatase activity, the phosphatase acts analogously to a co-receptor to lower the ligand off rates and boost apparent affinity up to ~100-fold.[26-27] Since the ligand recognition occurs exclusively within PYR1, the engineering of new CID modules can be highly simplified and can be exploited to design biosensors for diverse chemical classes. In our previous work, we produced several PYR1-derivatives that can selectively recognize various natural and synthetic cannabinoids;[28] and demonstrated that PYR1-derived receptors can be readily incorporated in ELISA-like assays to achieve sub-nM LODs in serum, saliva and diluted urine,[28] meeting the needs for detection of cannabinoids and SCs in clinical samples.[29,30]

However, the present ELISA-like assay needs multiple steps as well as several lengthy cycles of surface passivation and washing to remove non-specific interactions and reduce background, taking more than one day to complete. Interference of the matrix components was observed, leading to higher LODs in complex matrices than that obtained in the clean saline solution. To speed up detection and enhance assay sensitivity, we employ the superparamagnetic

nanorods modified with zwitterionic polymers (**ZIP**) for rapid detection of the natural and synthetic cannabinoids in various biospecimens, including saliva, serum, and urine, within 30 min. Detection of as low as 2.7 fM cannabinoid can be achieved in saliva, and LOD 10 – 1,000 times lower than reported previously is obtained in unprocessed biofluids.[31-37] Our detection platform should have great values for biomedical and clinical analyses of many different types of molecules of interest in addition to the natural and cannabinoids.

Experimental Section

Materials and Chemicals. The pooled human serum, saliva, and urine were purchased from Innovative Research. DNA probes used for protein immobilization were synthesized by Integrated DNA Technologies (IDT) (capture probe (**CP**): /5AmMC6/TT TTT TAA CGA CTC ATA TTA ACA A; and surface probe (**SP**): /5AmMC6/TT TTT TTG TTA ATA TGA GTC GTT). Δ^9-THC, CBDA, CP 47,497, 4F-MDMB, JWH-015, JWH-016, and WIN 55,212-2 were obtained from Cayman Chemical as DEA-exempt preparations where required.

Protein production. The recombinant PYR1 variants were expressed as 6×-His, 6×-His-maltose binding (MBP) or 6×-His- small ubiquitin-like modifier (SUMO) fusion proteins in *E. coli*, following procedures reported in previous works[38-40] and described in Supporting Information. They are: MBP-PYR1^{WIN}, His-PYR1^{4F}, SUMO-PYR1^{CBDA}, SUMO-PYR1^{THC}, SUMO-PYR1$^{JWH-015}$, SUMO-PYR1$^{JWH-016}$, and SUMO-PYR1 $^{CP47,\ 497}$. All recombinant proteins were purified as described in previous reported work.[38,40] In brief, sonicated lysates were purified using Ni-NTA agarose (Qiagen), and eluted proteins dialyzed against 1×Tris-Buffered Saline (TBS, 20 mM Tris, 150 mM NaCl).

Preparation and characterization of the zwitterionic polymer layers on nanorod surface. Synthesis of the silica coated superparamagnetic nanorods (Fe_3O_4@SiO_2 nanorods) followed the reported method;[41] and the steps for nanorod synthesis as well as for coating the nanorods with zwitterionic polymer layers can be found in Supporting Information. The as-prepared nanorods carrying different surface coatings were characterized with multiple techniques. Zeta potential measurements were performed in 1× PBS on a Zetasizer Advance Range (Malvern Analytical) using a folded capillary zeta cell. FT-IR measurements were done with a Nicolet iS50 FTIR Advanced KBr Gold Spectrometer. ^{1}H NMR spectra were recorded by a Bruker Avance NEO 400. Samples for transmission electron microscopy (TEM) were prepared by drying 10 μL of the diluted particle solution on the carbon-coated copper grids and imaged in the Thermo Scientific Talos L120C™ TEM after drying overnight. The X-ray photoelectron spectroscopy (XPS) was carried out on a Kratos Analytical AXIS Ultra Delay-Line Detector (DLD) Imaging XPS. Elemental analysis was carried out by the Oxford INCA Energy dispersive analytical system (EDS).

Coupling PYR1 and HAB1 variants with the capture probes. The CP modified-PYR1s were prepared via click reaction, with details described in Supporting Information, stored in a solution containing 10% vol/vol glycerol, 50 mM HEPES at pH 8.0, 200 mM KCl, 10 mM $MnCl_2$, 1 mM DTT, and 1 mM TCEP at -80 °C. The conjugates can be stable for more than 6 months under this storage condition, and was used without purification. They were captured on the surface probe (SP)-conjugated nanorod surface for drug detection via hybridization between CP and SP (Supporting Information).

Ligand/receptor-mediated protein phosphatase inhibition assay. In a typical inhibition assay, the MBP-PYR1^{WIN}-conjugated nanorods were dispersed in 10 μL of the assay buffer (100

mM Tris-HCl, 100 mM NaCl, 30 µg/mL BSA, 1 mM $MnCl_2$, and 0.1% 2-mercaptoethanol). Then, 2 µL of WIN 55,212-2, 5 µL of 2 µM catalytically active His-ΔN-HAB1, 143 µL of the assay buffer, and 40 µL of 5 mM 4-methylumbelliferyl phosphate were mixed and incubated at RT for 10 min on a stirrer. The fluorescence signal was recorded in the Synergy H1 Hybrid Multi-Mode Microplate Reader (BioTek). Alternatively, 5 µL of 2 µM MBP-$PYR1^{WIN}$ was used in the nanorod-free format, while keeping other conditions the same.

Nanorod-assisted ELISA-like assay. The nanorod-assisted ELISA-like assays were conducted using PYR1 variants and the catalytically inactive, thermo-stabilized MBP-ΔN-$HAB1^{T+}$.[28] In a typical assay, the PYR1-conjugated nanorods were dispersed in 10 µL of 1× CBSB (a solution containing 20 mM sodium citrate, 147 mM NaCl, 4.5 mM KCl, and 1% BSA), and incubated with 1 µL of the 10 µM biotinylated MBP-ΔN-$HAB1^{T+}$ and 1 µL of the cannabinoid target in different concentrations at RT on the magnetic stirrer for 15 min. After washing the nanorods with 1× CBSB three times, the nanorods were incubated with 10 µL of 0.05 µg/mL streptavidin- HRP prepared in 1× CBSB at RT on the stirrer for another 15 min. Finally, the nanorods were washed with 1× CBSB four times. Signal development was done by adding 100 µL of the SuperSignal West Pico PLUS Chemiluminescent Substrate and luminescence was read by the BioTek Synergy H1 Hybrid Multi-Mode Microplate Reader.

Results and Discussions

Design, fabrication, and characterization of the ZIP-coated nanorods. Slow molecular diffusion to the flat binding surface requires long incubation to ensure target capture, greatly elongating the ELISA-like assays.[28] To speed up target binding, we employed the superparamagnetic Fe_3O_4 nanorods with an ave. length × width of ~ 120 nm × 50 nm to be the

solid support for the protein receptors.[41] Besides being easily pulled down by an external magnet, they can rotate on a magnetic stirrer to enhance molecule diffusion, which should greatly speed up ligand capture by PYR1 derivatives and shorten assay duration. In addition, to enhance the sensitivity of drug detection in biofluids, we fabricated a stealth surface by coating the nanorods with the zwitterionic brush polymers of poly-CBMA. Zwitterionic polymers can form a stably bounded water layer around the polymer chains to prevent non-specific protein adsorption.[42] Poly-CBMA also contains rich carboxyl groups that can be used for bioconjugation. Moreover, we attempted a hierarchical polymer growth procedure to have the long and short polymer chains alternatively spaced on the nanorod surface, anticipating a loosely packed polymer layer could make the conjugation groups more accessible, reduce space hindrance and electrostatic repulsion, and thus enhance conjugation efficiency.

The major steps of the hierarchical growth of poly-CBMA on the nanorods are illustrated in **Figure 1a**. In brief, the silica surface of nanorods was firstly converted to primary amines via APTS treatment (**Step 1**) and then reacted with α-bromisobutylryl to bond with Br (**Step 2**), for polymerization initiation with the addition of CBMA, CuBr, and bpy (**Step 3**). After 16 h polymerization, the resultant nanorods referred as **nanorod-ZIP-Single Layer (SL)**, the reaction was terminated by addition of sodium azide (**Step 4**), which can cap some of the polymer chains by azide and leave others still terminated by Br to support the second round of polymer growth (**Step 5**). The product of the two-step polymerization was called **nanorod-ZIP-Dual Layer (DL)** to illustrate the presence of long- and short-chain polymers on nanorod surface.

The changes on nanorod surface at each synthesis step were characterized carefully. Zeta-potential measurements show that, while amine modification put positive charges on the initially negatively charged silica surface, substitution of the amine groups by Br neutralized the surface;

and growth of ZIP shifted the surface charges to negative because of its carboxyl groups, with ZIP-DL exhibiting a more negative potential than ZIP-SL because of the addition of more monomers, i.e. more carboxyl groups (**Fig. 1b**).

The atomic percentage (atomic%) of N and Br on the surface of nanorods isolated from each synthesis step was acquired by EDS (**Fig. 1c**). Br was persistently present on the surface after Step 2, with little change in its atomic% until a significant drop upon the completion of two-step polymer growth, i.e. Step 5. In contrast, the atomic% of N continuously increased in all subsequent steps, illustrating the growth of one polymer layer in Step 3, the addition of N_3 in Step 4, and the continuous polymer growth in Step 5. Agreeing with the reaction design, the ratio of Br/N reached the peak value at Step 2, the only step in which the precursor of α-bromisobutylryl was added, and kept decreasing with more and more N bonded to the surface.

Successful azide capping is critical to obtain the hierarchical polymer structure. We carried out XPS to examine the surface chemical composition on the nanorods resulted from Step 3, 4, & 5) **(Fig. 1d and Figure *S*-2)**. The N1s narrow scan (**Fig. 1d)** on nanorod-ZIP-SL exhibited two distinct peaks, representing the bond energy of C-N^+ (402.1 eV) and N-H (399.88 eV) on the monomer. Two additional peaks, 400.5 eV and 404.0 eV, showed up in the spectra of nanorod-ZIP-SL-N_3 and nanorod-ZIP-DL and have a peak area ratio of 2:1, proving the existence of the azide groups on the nanorod surface after completion of Step 4 and 5.[43-44] These results illustrate the hierarchical polymer growth in Step 3 and 5 from the Br reaction center, and the presence of N_3 on the surface since Step 4 that could have prevented further growth of some polymer chains to produce the DL coating.

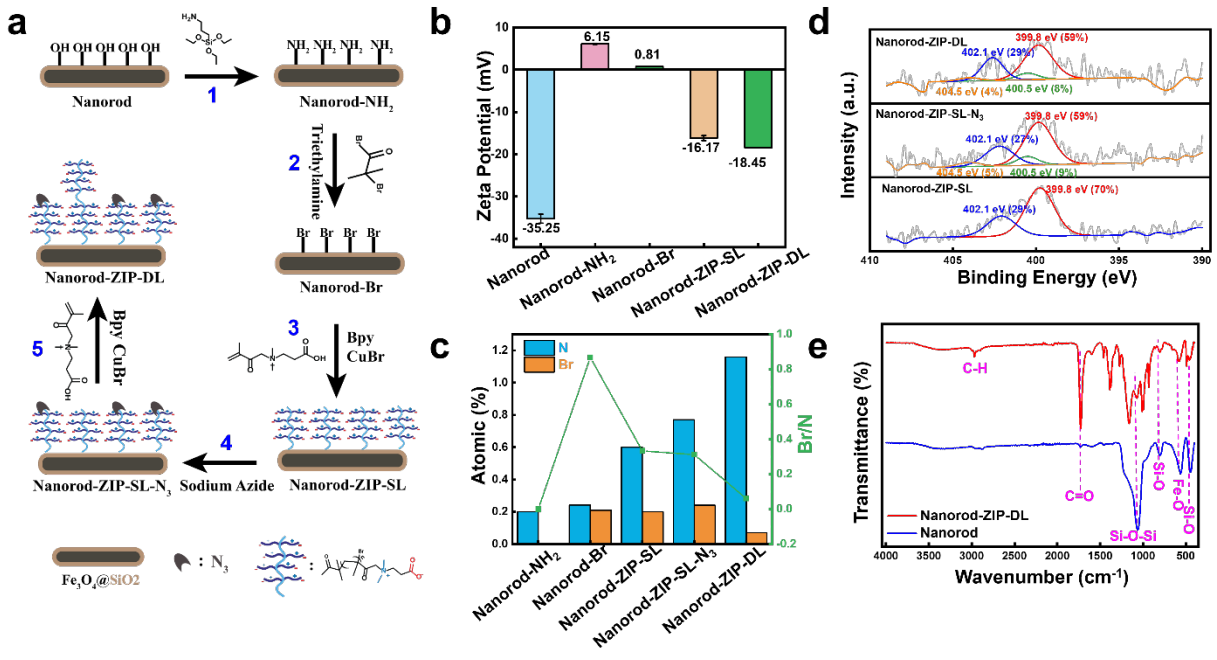

Figure 1. **Characterization of the zwitterionic polymer (ZIP) coating on nanorods. a)** The major steps for ZIP production via two-step polymerization on nanorods. **b)** Zeta potential comparison for the nanorods before polymer coating (Nanorod), and after modification with amines (Nanorod-NH_2), Br (Nanorod-Br), one-step (Nanorod-ZIP-SL) and two-step polymerization (Nanorod-ZIP-DL), all distributed in the 1× PBS. **c)** Elemental analysis and **d)** N1s deconvolution XPS spectra of the nanorod surface attained after each production step shown in **a)**. The peaks in **d)** at 400.5 eV and 404.0 eV with a ratio of 2:1 are characteristic for the azide group. **e)** FT-IR spectra of the chemical structures found on the nanorod before (blue) and after two-step polymerization (red).

The final coating produced by **Step 5** was examined by FT-IR (**Fig. 1e**). The characteristic band of Fe–O at 569 $cm^{-1}$was observed, as well as the significant absorption peaks for the asymmetric stretching, symmetric stretching, in-plane bending and rocking mode of Si–O–Si (1080, 945, 800, and 447 cm^{-1}), proving the integrity of the Fe_3O_4 core and the SiO_2 shell of the nanorods. Several distinct peaks at 1388 cm^{-1}, 1594 cm^{-1}, 1724 cm^{-1}, and 2973 cm^{-1}, were observed only on nanorod-ZIP-DL that respectively support the presence of CH_3 (2973 cm^{-1}),

C=O (stretching at 1724 cm^{-1}), and COO^- (symmetric stretching at 1388 cm^{-1} and asymmetric stretching at 1594 cm^{-1}) in poly-CBMA. TEM (**Supporting Figure *S*-1**) also confirmed that the polymerization did not alter the uniform core-shell rod structure of the nanorods and maintained their general dimensions to be ~120 nm long × 25 nm in diameter.

Zwitterionic feature, anti-fouling capability, and high conjugation efficiency of ZIP. The zwitterionic property of ZIP was confirmed by zeta-potential measurement (**Figure 2a**), and the isoelectric point of this polymer coating was found to be at pH 4.4. The ZIP surface would carry net negative charges in biofluids with pH between 5 and 7.5. The charge-induced repulsion could help the nanorods well suspended in sample and assay solutions.

The anti-fouling capability of ZIP was confirmed by evaluating the amounts of proteins adsorbed on the nanorods coated by ZIP-DL, PEG (Mw 350 Da), silica and silica modified with -NH_2 or –COOH, when incubated in undiluted human serum. The ZIP-DL surface yielded the lowest amount of protein adsorption, which is ~ 30% and 60% lower than that found on the PEG and unmodified silica surface, respectively (**Fig. 2b**) and more than 10× lower than the amine- or carboxyl-modified silica surface.

ZIP contains rich carboxyl groups; and the loosely packed polymer structure obtained from the two-step polymerization should make these functional groups highly accessible for bioconjugation, which would not affect the anti-fouling property.[45] In our design, the PYR1 proteins are immobilized on the ZIP-coated nanorods for target capture through DNA hybridization (**Fig. 2c**) between the SP conjugated to the nanorods and the CP to the PYR1. The resultant double-stranded DNA (dsDNA) provides sufficient flexibility and rigidity to serve as a cushion between the protein and the solid surface,[46] and help maintain the native structure of the conjugated protein.[47-48]

SP immobilization with different amounts of SP inputs with increasing SP input yielded more immobilized SP on the nanorod-ZIP; but more SP were conjugated on the nanorod-ZIP-DL, and the SP loadings on the PEG and ZIP-SL surfaces were comparable (**Supporting Information Figure *S*-3a&b**). These results prove that the two-step polymerization could produce the loosely packed polymer coating for improved accessibility of the functional groups and thus surface conjugation with biomolecules.

We also evaluated the amount of CP captured by the SP-modified nanorods via hybridization between SP and CP. With the conjugation condition that yielded 14 μg SP per mg nanorods, ZIP-DL outperformed ZIP-SL and PEG, capturing the highest amount (3.5 μg) of CP per unit mass of the nanorod (**Fig. 2d**). Since 1 mg of the nanorod contains ~ 10^{10} particles, a loading of 3.5 μg CP per mg nanorod means about 28,000 CP molecules were present on each nanorod, meaning that an equivalent amount of PYR1 can be immobilized on the nanorods. The high number of PYR1 on each nanorod should facilitate rapid drug binding and high binding capacity. However, increasing SP loading on the nanorods further did not yield more CP to be captured (**Fig. *S*-*3c***), probably the strong electrostatic repulsion between the negatively charged DNA chains preventing CP from approaching to the nanorod surface for SP hybridization.

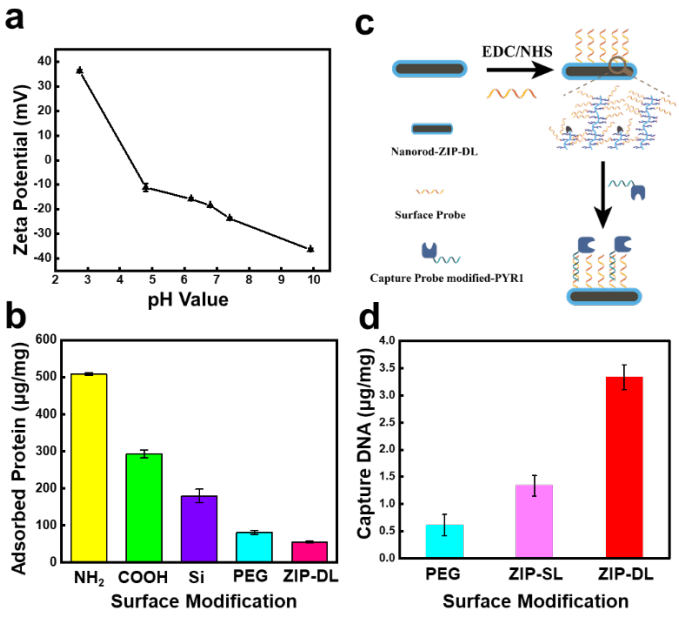

Figure 2. **Unique features of the ZIP coating. a)** Zeta potential of nanorod-ZIP-DL measured at different pH values. **b)** Comparison of the amount of proteins non-specifically adsorbed on 1 mg of the nanorods carrying different types of surface coating. **c)** Schematic illustration of SP conjugation by EDC/NHS on the ZIP-DL-coated nanorods, and immobilization of the capture probe (CP)-conjugated PYR1 through DNA hybridization between SP and CP. **d)** Comparison of the amount of CP immobilized on 1 mg of the nanorods carrying PEG, ZIP-SL, or ZIP-DL as the surface coating.

Phosphatase inhibition enhanced by nanorods for ultrafast drug detection. The phosphatase activity of HAB1 is inhibited upon dimer formation with PYR1 in the presence of durgs. This feature, in conjunction with a fluorogenic phosphatase substrate, can be utilized to design a simple phosphatase inhibition assay for cannabinoid detection. Thus, we tested the performance of such an assay with the PYR1 immobilized on the nanorods. Our published work found that MBP-PYR1^{WIN} displayed a half-maximum effective concentration (EC_{50}) value of 72 nM towards (+)-WIN 55,212-2 (henceforth referred to as **WIN**) using the protein phosphatase inhibition assay.[38] We herein chose MBP-PYR1^{WIN} for proof-of-principle studies, and

conjugated it with the CP for immobilization on the nanorods. Our conjugation condition loaded 3-5 DBCO molecules per receptor, which should be equivalent to the number of CP conjugated to each PYR1 (**Supporting Information Figure *S*-4**).

We found that the activity of His-ΔN-HAB1, the catalytically active HAB1 N-terminal deletion mutant, could be impacted by either physical adsorption or covalent conjugation to the nanorods, but not by modification with small molecules like biotin, DBCO, and ssDNA (**Supporting Information Figure S-5**). The inhibitory effect of the nanorods to the phosphatase may help enhance signal changes in the phosphatase assay: with the ZIP-DL coating on the nanorods to minimize the nonspecific adsorption of His-ΔN-HAB1, only the specific drug-binding events can bring His-ΔN-HAB1 in close proximity to the nanorods, with its activity reduced by both CID and the nanorods.

Herein, we prepared the MBP-PYR1^{WIN}-conjugated nanorods-ZIP-DL through hybridization between the CP on the MBP-PYR1^{WIN} and the SP on the nanorods to conduct the phosphatase inhibition assay. The resultant nanorods were mixed with 5 μM His-ΔN-HAB1 and WIN at concentrations from 10 pM to 10 μM. The fluorescent signals continuously dropped with increasing WIN concentration, and a faster decrease with unit increase of the drug concentration was observed with the nanorod-supported assay compared to the in-solution assay (**Figure 3**), which also yielded an LOD 100× lower. This assay permits ultrafast (taking only 10 min) and simple detection of cannabinoids down to 100 pM for real-world applications, because the regulatory guideline of cannabinoids is 3 nM for WIN.[49]

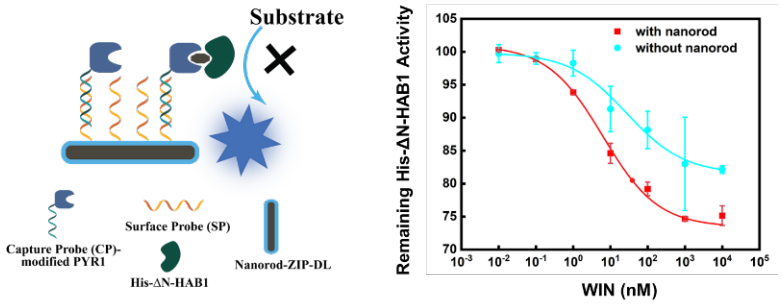

Figure 3. **Phosphatase inhibition assay.** Titration curves of the ligand-dependent phosphatase inhibition assay performed on the nanorods coated by ZIP-DL (red) or in solution (blue).

Ultrasensitive cannabinoid detection by the nanorod-assisted ELISA-like assay. To achieve even greater sensitivity in cannabinoid detection, we developed the nanorod-assisted ELISA-like assay, in which the drug is initially captured by the receptor-conjugated nanorods, and then the biotinylated but catalytically inactive MBP-ΔN-HAB1^{T+} is added to capture the streptavidin-HRP for chemiluminescence (CL) production (**Figure 4a**).

The calibration curves obtained by using nanorods carrying different surface coatings (PEG, ZIP-SL, and ZIP-DL) for the detection of WIN in saline are shown in **Figure 4b and Supporting Figure S6**. The ZIP surface exhibited significantly higher CL compared to PEG, and the signals generated on nanorod-ZIP-DL were ~ 1.5 times higher than those from ZIP-SL, owing to the higher receptor loading enabled by the double-layer ZIP. Remarkably, when compared to assays performed on the conventional multi-well plates, the nanorod-based assays achieved a much lower LOD and a significantly larger dynamic range. In particular, the lowest detectable drug concentration obtained with nanorod-ZIP-DL was 0.01 pM, with the LOD calculated to be 0.001 pM using the 3σ method; and the dynamic range covered over 9 orders of magnitude. This LOD is 10,000× lower and the dynamic range is 6 orders of magnitude wider

than the corresponding values reported in our published work that employed the same PYR1/MBP-ΔN-HAB1^{T+} pair in a 96-well plate and the colorimetric substrate of HRP for signal development (the detection results for such an assay using the CL signaling method were worse than absorption detection due to high background and high signal variation (**Supporting Information Figure S7**)).[28] Such an LOD is also much lower than the methods reported so far in literature for detection of cannabinoids or other controlled drugs (**Table S1**);[31-37]and our dynamic range is 2-3 orders of magnitude wider than that obtained with the powerful techniques of SIMOA or nanomaterial-based signal amplification for biomarker detection.[50-52]

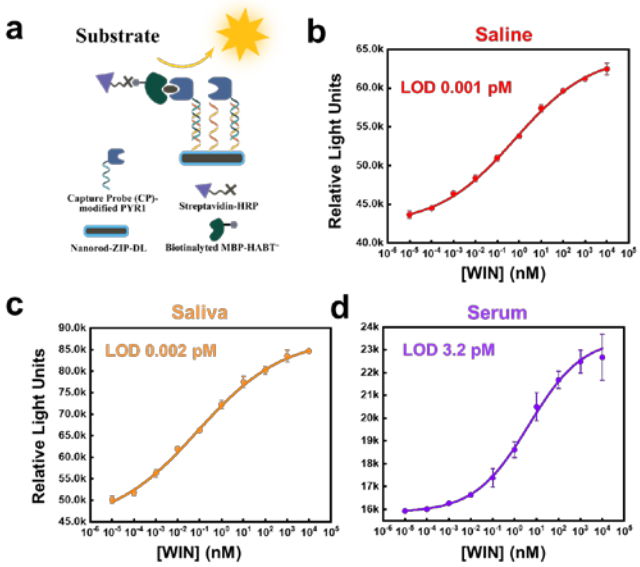

Figure 4. **Nanorod-assisted ELISA-like assay. a)** Scheme of the assay: immobilized receptors recruit biotinylated MBP-ΔN-HAB1^{T+} in response to ligand, and a CL signal is generated by a secondary streptavidin-HRP conjugate. WIN detection in saline **b)**, undiluted human saliva **c)**, and serum **d)** assisted by nanorod-ZIP-DL. The blank in saline, saliva, and serum was 4017±997, 34700±83 and 12523±122, separately. Each data point represents the mean of three replicates, with the error bar representing the standard deviation. The LOD was calculated via the 3σ method, equivalent to the drug concentration that would give out a signal equal to 3 times of the standard deviation of the blank after blank subtraction.

Furthermore, the anti-fouling capability of ZIP enables sensitive drug detection in various complex matrices (**Fig. 4c-d and Supporting Figure S8d**). In contrast to the conventional multi-well plate surface, where detection performance declines substantially in diluted complex matrices, the nanorod-ZIP-DL maintained excellent detection performance in undiluted biofluids. In saliva, the LOD was calculated to be 0.002 pM, comparable to that in saline. Although PEG also demonstrated good anti-fouling performance (**Figure S-8a-c**), nanorod-ZIP-DL delivered LODs 5-10 times lower, especially in urine and serum, reaching 1.37 pM in urine and 3.2 pM in serum.

The poorer detection performance found in serum and urine than in salvia could be attributed to their different matrix compositions. Serum contains 3-5 mg/mL albumin that can sequester small molecular drugs and substantially reduce the concentrations of free drugs for PYR1 binding. Urine always exhibits very high background signals when using the PYR1 system for drug detection, probably due to its rich content of metabolites[53] that may compete with cannabinoids for PYR1 binding via non-specific interaction. Normal saliva contains only ~ 0.5 – 2 mg/mL total proteins,[54] most of which are salivary proteins with no affinity for drugs, thus exhibits the least matrix impact for cannabinoid detection.

Multiplex detection of cannabinoids. Our previous work successfully developed 14 PYR1 mutants with specific binding capabilities to various natural and synthetic cannabinoids. Thus, we tested in detail the performance of two more receptors, SUMO-PYR1^{THC} and SUMO-PYR1^{CBDA}, in the detection of their corresponding targets, Δ9-THC and CBDA, on the nanorod platform. We found that, Δ9-THC could be detected with LODs of 0.019 pM in saline and 0.76 pM in saliva, and CBDA detection yielded LODs of 20 pM in saline and 17 pM in saliva, both

showing a wide dynamic range extending up to 10 µM (**Supporting Information Figure S-9**). These LODs are not as low as that of WIN, probably due to the lower affinity of these receptors to their target drugs compared to MBP-PYR1^{WIN}. Still, they are more than sufficient for the detection of recent drug exposure.

We further assessed the detection specificity in two ways. Firstly, we compared the CL signal generated by the MBP-PYR1^{WIN}-conjugated nanorod-ZIP-DL when incubated with different drugs at the same concentration. The CL signal generated by the positive target, WIN, was more than four times higher than those produced by other drugs (**Figure 5a**). Secondly, we tested the detection of the target drug in the presence of five other drugs using the nanorods conjugated with the corresponding receptor. For example, WIN detection by the MBP-PYR1^{WIN}-conjugated nanorod-ZIP-DL was performed in a solution containing WIN (positive target) and five other drugs (negative targets) mixed at 1 µM each, and the positive signal was compared to that produced by the mixture of the five "negative" targets. All of the receptors tested produced positive signals 2 to 4 times higher than that obtained without the target drug (**Fig. 5b**). One exception was His-PYR1^{4F}, which responded to the negative targets more strongly than to the tested receptors. His-PYR1^{4F} showed little cross-reactivity even at high concentrations of WIN when tested in the yeast two-hybrid system or *in vitro* using the ELISA-like assay in multi-well plates and MBP-PYR1^{4F}.[28] However, using the ssDNA-modified His-PYR1^{4F} in our assays, we observe cross-reactivity with WIN, JWH-016, and THC (**Supporting Information Figure S-10a**). This suggests that tag choice may alter receptor performance and that MBP or SUMO tags are preferable to use over only a 6x-His-tag. For the MBP and SUMO-tagged receptors, their signal intensity obtained in our assays is positively correlated with the binding affinity reported

previously, indicating a good correlation between sensing performance and receptor-drug binding affinity found in the cell-based screening system (**Fig. S10b**).

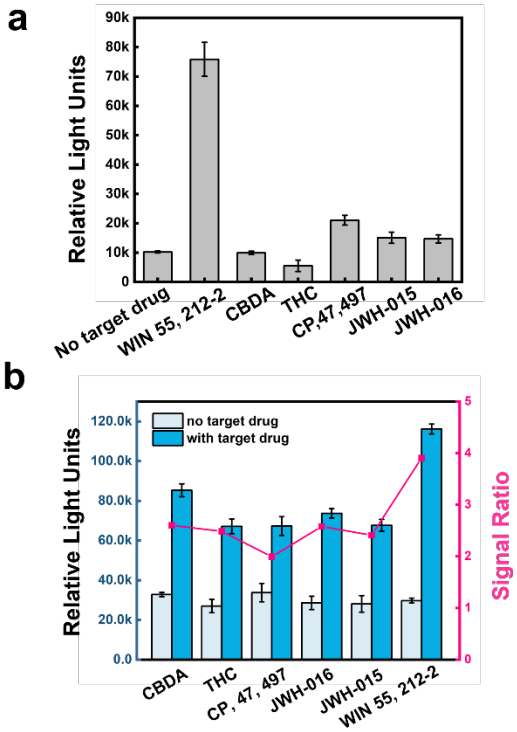

Figure 5. **Specificity of the nanorod-assisted ELISA-like assay in cannabinoid detection. a)** Comparison of CL signals produced by 1 μM of WIN, THC, CBDA, JWH-015, JWH-016, CP47, 497, or 4F-MDMB distributed in saline, using the receptor of MBP-PYR1^{WIN}. **b)** Bar plots comparing the CL signals generated from the drug mixtures with or without the target drugs, and the curve showing the ratios of the positive (with the target drug) vs. negative (without the target drug) signals. Each drug in the mixture was at 1 μM. Receptors employed in this experiment were MBP-PYR1^{WIN}, His-PYR1^{4F}, SUMO-PYR1^{CBDA}, SUMO-PYR1^{THC}, SUMO-PYR1$^{JWH-015}$, SUMO-PYR1$^{JWH-016}$, SUMO-PYR1$^{CP47, 497}$. The results were the average value and the standard deviation (error bar) from three replicates.

Conclusion

In this study, we fabricated the magnetic nanorods coated with a hierarchical double-layer zwitterionic polymer and demonstrated their impressive capability in enhancing the performance of employing plant hormone receptors for cannabinoid detection. Such a sensor platform can improve molecular diffusion for efficient target capture and fast as well as sensitive drug detection. The hierarchical polymer growth produce the loosely packed ZIP layers, delivering high capacity for conjugation of the drug recognition units and minimizing non-specific protein adsorption for improved signal-to-noise ratios when detecting in undiluted biofluids. Irrespective of the specific method employed, our study showcases the significantly enhanced sensing performance when using the ZIP-coated nanorods as the solid support in the immunoassay-like methods. This sensing platform should also be suitable for employment of a high number of rapidly produced receptors using the high-density mutagenesis PYR1-HAB1 system for detection of small molecules of interest.

ASSOCIATED CONTENT

Supporting Information

Additional method description, nanorod characterization (results from TEM, XPS), ^{1}H NMR of CBMA, primers used in SUMO protein expression and sequences of fusion proteins MBP and SUMO, surface modification comparison (capture efficiency, loading efficiency, non-specific adsorption), protein conjugation and its effect on protein activity, and cannabinoid detection performance. This material is available free of charge via the Internet at http://pubs.acs.org.

Author Information

Corresponding Author

* E-mail: wenwan.zhong@ucr.edu

Acknowledgements

The research work was supported by the National Institutes of Health/National Institute on Drug Abuse (grant 1R21DA053496-01 to S.R.C and W.Z.) and the National Science Foundation (NSF- 2128287 to T.A.W., grant NSF-2128016 to S.R.C. and I.W.).

Reference

(1) *https://www.unodc.org/unodc/en/data-and-analysis/world-drug-report-2022.html*.

(2) Bhunia, S.; Kolishetti, N.; Arias, A. Y.; Vashist, A.; Nair, M. Cannabidiol for neurodegenerative disorders: a comprehensive review. *Front. Pharmacol.* **2022**, *13*, 989717.

(3) Silva-Reis, R.; Silva, A. M. S.; Oliveira, P. A.; Cardoso, S. M. Antitumor Effects of Cannabis sativa Bioactive Compounds on Colorectal Carcinogenesis. *Biomolecules* **2023**, *13*, 764.

(4) Giorgetti, A.; Orazietti, V.; Busardò, F. P.; Giorgetti, R. Psychomotor performances relevant for driving under the combined effect of ethanol and synthetic cannabinoids: A systematic review. *Front. Psychiatry.* **2023**, *14*, 1131335.

(5) Scopetti, M.; Morena, D.; Manetti, F.; Santurro, A.; Fazio, N. D.; D′Errico, S.; Padovano, M.; Frati, P.; Fineschi, V. Cannabinoids and Brain Damage: A Systematic Review on a Frequently Overlooked Issue. *Curr. Pharm. Biotechnol.* **2023**, *24*, 741-757.

(6) Hines, L. A.; Freeman, T. P.; Gage, S. H.; Zammit, S.; Hickman, M.; Cannon, M.; Munafo, M.; MacLeod, J.; Heron, J. Association of High-Potency Cannabis Use With Mental Health and Substance Use in Adolescence. *JAMA Psychiatry* **2020**, *77*, 1044-1051.

(7) Tait, R. J.; Caldicott, D.; Mountain, D.; Hill, S. L.; Lenton, S. A systematic review of adverse events arising from the use of synthetic cannabinoids and their associated treatment. *Clin. Toxicol.* **2016**, *54*, 1-13.

(8) Cohen, K.; Weinstein, A. M. Synthetic and Non-synthetic Cannabinoid Drugs and Their Adverse Effects-A Review From Public Health Prospective. *Front. public health* **2018**, *6*, 162.

(9) Klimuntowski, M.; Alam, M. M.; Singh, G.; Howlader, M. M. R. Electrochemical Sensing of Cannabinoids in Biofluids: A Noninvasive Tool for Drug Detection. *ACS Sens* **2020**, *5*, 620-636.

(10) Grotenhermen, F. Pharmacokinetics and Pharmacodynamics of Cannabinoids. *Clin. Pharmacokinetics* **2003**, *42*, 327-360.

(11) Huestis, M. A.; Henningfield, J. E.; Cone, E. J. Absorption of THC and formation of 11-OH-THC and THCCOOH during and after smoking marijuana. *J. Anal. Toxicol.* **1992**, *16*, 276-282.

(12) Gjerde, H.; Beylich, K. M.; Morland, Incidence of alcohol and drugs in fatally injured car drivers in Norway. J. *Accid. Anal. Prev.* **1993**, *25*, 479-483.

(13) Sim, Y. E.; Kim, J. W.; Ko, B. J.; Kim, J. Y.; Cheong, J. C.; Pyo, J. Determination of urinary metabolites of cannabidiol, Δ8-tetrahydrocannabinol, and Δ9-tetrahydrocannabinol by automated online μSPE-LC-MS/MS method. *J. Chromatogr. B: Anal. Technol. Biomed. Life Sci.* **2023**, *1214*, 123568.

(14) Typek, R.; Holowinski, P.; Dawidowicz, A. L.; Dybowski, M. P.; Rombel, M. Chromatographic analysis of CBD and THC after their acylation with blockade of compound transformation. *Talanta* **2023**, *251*, 123777.

(15) Moody, M. T.; Ringel, M. M.; Mathews, C. M.; Midthun, K. M. Determination of Cross-Reactivity of Contemporary Cannabinoids with THC Direct Immunoassay (ELISA) in Whole Blood. *J. Anal. Toxicol.* **2022**, *46*, 844-851.

(16) Sempio, C.; Wymore, E.; Palmer, C.; Bunik, M.; Henthorn, T. K.; Christians, U.; Klawitter, J. Detection of Cannabinoids by LC–MS-MS and ELISA in Breast Milk. *J. Anal. Toxicol.* **2021**, *45*, 686-692.

(17) Cannaert, A.; Ramirez Fernandez, M. D. M.; Theunissen, E. L.; Ramaekers, J. G.; Wille, S. M. R.; Stove, C. P. Semiquantitative Activity-Based Detection of JWH-018, a Synthetic Cannabinoid Receptor Agonist, in Oral Fluid after Vaping. *Anal. Chem.* **2020**, *92*, 6065-6071.

(18) Cannaert, A.; Storme, J.; Hess, C.; Auwarter, V.; Wille, S. M. R.; Stove, C. P. Activity-Based Detection of Cannabinoids in Serum and Plasma Samples. *Clin. Chem.* **2018**, *64*, 918-926.

(19) Lu, D.; Lu, F.; Pang, G. A Novel Tetrahydrocannabinol Electrochemical Nano Immunosensor Based on Horseradish Peroxidase and Double-Layer Gold Nanoparticles. *Molecules* **2016**, 21(10), 1377.

(20) Martinez-Perez-Cejuela, H.; Conejero, M.; Amoros, P.; El Haskouri, J.; Simo-Alfonso, E. F.; Herrero-Martinez, J. M.; Armenta, S. Metal-organic frameworks as promising solid-phase sorbents for the isolation of third-generation synthetic cannabinoids in biological samples. *Anal. Chim. Acta* **2023**, *1246*, 340887.

(21) Moorthy, G. S.; Vedar, C.; DiLiberto, M. A.; Zuppa, A. F. A patient-centric liquid chromatography-tandem mass spectrometry microsampling assay for analysis of cannabinoids in

human whole blood: Application to pediatric pharmacokinetic study. *J. Chromatogr. B: Anal. Technol. Biomed. Life Sci.* **2019**, *1130-1131*, 121828.

(22) Balaban, S.; Man, E.; Durmus, C.; Bor, G.; Ceylan, A. E.; Gumus, Z. P.; Evran, S.; Coskunol, H.; Timur, S. Sensor Platform with a Custom-Tailored Aptamer for Diagnosis of Synthetic Cannabinoids. *Electroanal.* **2020**, *32*, 656-665.

(23) Yu, H. X.; Luo, Y. P.; Alkhamis, O.; Canoura, J.; Yu, B. Y.; Xiao, Y. Isolation of Natural DNA Aptamers for Challenging Small-Molecule Targets, Cannabinoids. *Anal. Chem.* **2021**, *93*, 3172-3180.

(24) Mascini, M.; Montesano, C.; Perez, G.; Wang, J.; Compagnone, D.; Sergi, M. Selective solid phase extraction of JWH synthetic cannabinoids by using computationally designed peptides. *Talanta* **2017**, *167*, 126-133.

(25) Park, S. Y.; Peterson, F. C.; Mosquna, A.; Yao, J.; Volkman, B. F.; Cutler, S. R. Agrochemical control of plant water use using engineered abscisic acid receptors. *Nature* **2015**, *520*, 545-548.

(26) Ma, Y.; Szostkiewicz, I.; Korte, A.; Moes, D.; Yang, Y.; Christmann, A.; Grill, E. Regulators of PP2C Phosphatase Activity Function as Abscisic Acid Sensors. *Science* **2009**, *324*, 1064-1068.

(27) Szostkiewicz, I.; Richter, K.; Kepka, M.; Demmel, S.; Ma, Y.; Korte, A.; Assaad, F. F.; Christmann, A.; Grill, E. Closely related receptor complexes differ in their ABA selectivity and sensitivity. *Plant J.* **2010**, *61*, 25-35.

(28) Beltran, J.; Steiner, P. J.; Bedewitz, M.; Wei, S.; Peterson, F. C.; Li, Z. B.; Hughes, B. E.; Hartley, Z.; Robertson, N. R.; Medina-Cucurella, A. V.; Baumer, Z. T.; Leonard, A. C.; Park, S. Y.; Volkman, B. F.; Nusinow, D. A.; Zhong, W. W.; Wheeldon, I.; Cutler, S. R.; Whitehead, T.

A. Rapid biosensor development using plant hormone receptors as reprogrammable scaffolds. *Nat. Biotechnol.* **2022**, *40*.

(29) Peterson, B. L.; Couper, F. J. Concentrations of AB-CHMINACA and AB-PINACA and Driving Behavior in Suspected Impaired Driving Cases. *J. Anal. Toxicol.* **2015**, *39*, 642-647.

(30) Hutchison, R. D.; Ford, B. M.; Franks, L. N.; Wilson, C. D.; Yarbrough, A. L.; Fujiwara, R.; Su, M. K.; Fernandez, D.; James, L. P.; Moran, J. H.; Patton, A. L.; Fantegrossi, W. E.; Radominska-Pandya, A.; Prather, P. L. A typical Pharmacodynamic Properties and Metabolic Profile of the Abused Synthetic Cannabinoid AB-PINACA: Potential Contribution to Pronounced Adverse Effects Relative to Δ(9)-THC. *Front. Pharmacol.* **2018**, *9*, 1084.

(31) Plouffe, B. D.; Murthy, S. K. Fluorescence-based lateral flow assays for rapid oral fluid roadside detection of cannabis use. *Electrophoresis* **2017**, *38*, 501-506.

(32) Emrani, A. S.; Danesh, N. M.; Ramezani, M.; Taghdisi, S. M.; Abnous, K. A novel fluorescent aptasensor based on hairpin structure of complementary strand of aptamer and nanoparticles as a signal amplification approach for ultrasensitive detection of cocaine. *Biosens. Bioelectron.* **2016**, *79*, 288-293.

(33) Durmus, H.; Durmazel, S.; Uzer, A.; Gokdere, B.; Ercag, E.; Apak, R. A novel fluorescent aptasensor based on hairpin structure of complementary strand of aptamer and nanoparticles as a signal amplification approach for ultrasensitive detection of cocaine. *Anal. Sci.* **2018**, *34*, 1419-1425.

(34) Sivashanmugan, K.; Squire, K.; Tan, A. L.; Zhao, Y.; Kraai, J. A.; Rorrer, G. L.; Wang, A. X. Trace Detection of Tetrahydrocannabinol in Body Fluid via Surface-Enhanced Raman Scattering and Principal Component Analysis. *Acs Sensors* **2019**, *4*, 1109-1117.

(35) Xue, W.; Tan, X. T.; Oo, M. K. K.; Kulkarni, G.; Ilgen, M. A. A.; Fan, X. D. Rapid and sensitive detection of drugs of abuse in sweat by multiplexed capillary based immuno-biosensors. *Analyst* **2020**, *145*, 1346-1354.

(36) Pholsiri, T.; Lomae, A.; Pungjunun, K.; Vimolmangkang, S.; Siangproh, W.; Chailapakul, O. A chromatographic paper-based electrochemical device to determine Delta(theta)-tetrahydrocannabinol and cannabidiol in cannabis oil. *Sensor Actuat. B-Chem.* **2022**, *355*.

(37) Solin, K.; Vuoriluoto, M.; Khakalo, A.; Tammelin, T. Cannabis detection with solid sensors and paper-based immunoassays by conjugating antibodies to nanocellulose. *Carbohyd. Polym.* **2023**, *304*.

(38) Vaidya, A. S.; Helander, J. D. M.; Peterson, F. C.; Elzinga, D.; Dejonghe, W.; Kaundal, A.; Park, S. Y.; Xing, Z. N.; Mega, R.; Takeuchi, J.; Khanderahoo, B.; Bishay, S.; Volkman, B. F.; Todoroki, Y.; Okamoto, M.; Cutler, S. R. Dynamic control of plant water use using designed ABA receptor agonists. *Science* **2019**, *366*, eaaw8848.

(39) Steiner, P. J.; Bedewitz, M. A.; Medina-Cucurella, A. V.; Cutler, S. R.; Whitehead, T. A. A yeast surface display platform for plant hormone receptors: Toward directed evolution of new biosensors. *Aiche. J.* **2020**, *66*, e16767.

(40) Vaidya, A. S.; Peterson, F. C.; Yarmolinsky, D.; Merilo, E.; Verstraeten, I.; Park, S.-Y.; Elzinga, D.; Kaundal, A.; Helander, J.; Lozano-Juste, J.; Otani, M.; Wu, K.; Jensen, D. R.; Kollist, H.; Volkman, B. F.; Cutler, S. R. A Rationally Designed Agonist Defines Subfamily IIIA Abscisic Acid Receptors As Critical Targets for Manipulating Transpiration. *ACS Chem. Biol.* **2017**, *12*, 2842-2848.

(41) Li, Z. W.; Jin, J. B.; Yang, F.; Song, N. N.; Yin, Y. D. Coupling magnetic and plasmonic anisotropy in hybrid nanorods for mechanochromic responses. *Nat. Commun.* **2020**, *11*.

(42) Zhang, Y. X.; Liu, Y. L.; Ren, B. P.; Zhang, D.; Xie, S. W.; Chang, Y.; Yang, J. T.; Wu, J.; Xu, L. J.; Zheng, J. Fundamentals and applications of zwitterionic antifouling polymers. *J. Phys. D. Appl. Phys.* **2019**, *52*.

(43) Lin, Y. M.; Wang, L.; Zhou, J. S.; Ye, L.; Hu, H. Y.; Luo, Z. K.; Zhou, L. Surface modification of PVA hydrogel membranes with carboxybetaine methacrylate via PET-RAFT for anti-fouling. *Polymer* **2019**, *162*, 80-90.

(44) Liu, W. J.; Li, C.; Ren, Y. J.; Sun, X. B.; Pan, W.; Li, Y. H.; Wang, J. P.; Wang, W. J. Carbon dots: surface engineering and applications. *J. Mater. Chem. B* **2016**, *4*, 5772-5788.

(45) Vaisocherova, H.; Yang, W.; Zhang, Z.; Cao, Z. Q.; Cheng, G.; Piliarik, M.; Homola, J.; Jiang, S. Y. Ultralow fouling and functionalizable surface chemistry based on a zwitterionic polymer enabling sensitive and specific protein detection in undiluted blood plasma. *Anal. Chem.* **2008**, *80*, 7894-7901.

(47) Seymour, E.; Daaboul, G. G.; Zhang, X. R.; Scherr, S. M.; Unlu, N. L.; Connor, J. H.; Unlu, M. S. DNA-Directed Antibody Immobilization for Enhanced Detection of Single Viral Pathogens. *Anal. Chem.* **2015**, *87*, 10505-10512.

(47) Leidner, A.; Bauer, J.; Khonachah, M. E.; Takamiya, M.; Strahle, U.; Dickmeis, T.; Rabe, K. S.; Niemeyer, C. M. Oriented immobilization of a delicate glucose-sensing protein on silica nanoparticles. *Biomaterials* **2019**, *190*, 76-85.

(48) Jia, F.; Narasimhan, B.; Mallapragada, S. Materials-Based Strategies for Multi-Enzyme Immobilization and Co-Localization: A Review. *Biotechnol. Bioeng.* **2014**, *111*, 209-222.

(49) Yu, H.; Lee, H.; Cheong, J.; Woo, S. W.; Oh, J.; Oh, H. K.; Lee, J. H.; Zheng, H.; Castro, C. M.; Yoo, Y. E.; Kim, M. G.; Cheon, J.; Weissleder, R.; Lee, H. A rapid assay provides on-site quantification of tetrahydrocannabinol in oral fluid. *Sci. Transl. Med.* **2021**, *13*, eabe2352.

(50) Rissin, D. M.; Fournier, D. R.; Piech, T.; Kan, C. W.; Campbell, T. G.; Song, L. A.; Chang, L.; Rivnak, A. J.; Patel, P. P.; Provuncher, G. K.; Ferrell, E. P.; Howes, S. C.; Pink, B. A.; Minnehan, K. A.; Wilson, D. H.; Duffy, D. C. Simultaneous Detection of Single Molecules and Singulated Ensembles of Molecules Enables Immunoassays with Broad Dynamic Range. *Anal. Chem.* **2011**, *83*, 2279-2285.

(51) Sanjay, S. T.; Li, M. H.; Zhou, W.; Li, X. C.; Li, X. J. A reusable PMMA/paper hybrid plug-and-play microfluidic device for an ultrasensitive immunoassay with a wide dynamic range. *Microsyst Nanoeng* **2020**, *6*.

(52) Loynachan, C. N.; Thomas, M. R.; Gray, E. R.; Richards, D. A.; Kim, J.; Miller, B. S.; Brookes, J. C.; Agarwal, S.; Chudasama, V.; McKendry, R. A.; Stevens, M. M. Platinum Nanocatalyst Amplification: Redefining the Gold Standard for Lateral Flow Immunoassays with Ultrabroad Dynamic Range. *Acs Nano* **2018**, *12*, 279-288.

(53) Sarigul, N.; Korkmaz, F.; Kurultak, İ. A New Artificial Urine Protocol to Better Imitate Human Urine. *Sci. Rep.* 2019, 9, 20159.

(54) Mohamed, R.; Campbell, J.-L.; Cooper-White, J.; Dimeski, G.; Punyadeera, C. The impact of saliva collection and processing methods on CRP, IgE, and Myoglobin immunoassays *Clin. Transl. Med.* 2012, 1, 19.

For Table of Contents Only

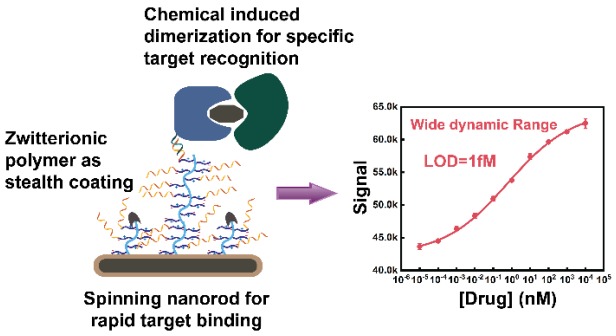

A High-Performance Cannabinoid Sensor Empowered by Plant Hormone Receptors and Antifouling Magnetic Nanorods

Zongbo Li,[1] Yuyang Shen,[2] Jesús Beltrán,[3,4] Hao Tian[3,4], Matthew Bedewitz[6], Ian Wheeldon,[4,5] Timothy A. Whitehead,[6] Sean R. Cutler[3, 4] and Wenwan Zhong[1, 2, *]

[1]Department of Chemistry; [2]Environmental Toxicology Graduate Program; [3]Department of Botany and Plant Sciences; [4]Institute for Integrative Genome Biology; [5]Department of Chemical and Environmental Engineering, University of California-Riverside, Riverside, CA 92521, U.S.A.

[6]Department of Chemical and Biological Engineering, University of Colorado Boulder, Boulder, CO, USA.

* Corresponding author

Wenwan Zhong, email: wenwan.zhong@ucr.edu

Supporting Information

Table of Contents

1. **Supplemental Materials and Methods** S-3
2. **Nanorod characterization** S-5
3. **Difference Surface Modification Comparison** S-7
4. **PYR1 and HAB1 Conjugation** S-8
5. **Cannabinoid detection performance** S-9
6. **^{1}H NMR** S-11
7. **Comparison table with techniques reported ……** S-12
8. **References** S-12

1. Supplemental Materials and Methods

Materials and Chemicals. Iron(III) chloride hexahydrate ($FeCl_3 \cdot 6H_2O$, 99+%, extra pure) and tetraethyl orthosilicate (TEOS) were obtained from Acros Organics. Poly(acrylic acid) (PAA ~1,800), (3-aminopropyl)triethoxysilane (APTES), triethylamine, 2,2'-bipyridine (bpy), copper(I) bromide (CuBr, 98%), α-bromoisobutyryl bromide (BIBB, 98%), 2-(dimethylamino)ethyl methacrylate (DMEM), HEPES, potassium chloride, 1,4-dithiothreitol (DTT), and 4-methylumbelliferyl phosphateand triethylene glycol (TEG) were purchased from Sigma Aldrich. N-hydroxysuccinimide (NHS), 1-ethyl-3-(-3-dimethylaminopropyl) carbodiimide hydrochloride (EDC), EZ Link Sulfo-NHS-LC-Biotin, phosphate buffered saline (PBS) (10× solution, molecular biology grade), manganese chloride tetrahydrate and Micro BCA™ Protein Assay Kit were acquired from ThermoFisher Scientific. N,N-dimethylformamide (DMF) was from EMD Millipore. β-propiolactone was obtained from the Alfa Aesar, respectively. Glycerol and mPEG-NH_2 was from Promega and Abbexa, respectively. DBCO-$(PEG)_5$-NHS ester and azido-$(PEG)_4$-NHS were purchased from Click Chemistry Tools. Streptavidin horseradish peroxidase (HRP) was purchased from Cepham Life Sciences.

Synthesis of nanorods. Firstly, 10.8 g of $FeCl_3.6H_2O$ was dissolved in 400 mL deionized water (DI water) and incubated at 87 °C for 18 hours (h) without any disturbance. The precipitation was collected and washed with DI water three times at 11,000 rpm. The obtained FeOOH rods were dispersed in 40 mL DI water. To coat the FeOOH with SiO_2, the FeOOH rods were modified with PAA firstly via incubating 10 mL FeOOH with 216 mg of PAA (Mw ~1,800) in 600 mL of DI water overnight under the stirring condition. The PAA-modified FeOOH was washed with DI water three times at 11,000 rpm for 15 minutes and dispersed in 12 mL DI water. For the silica coating, 150 µl TEOS was added to a mixture containing 2 mL of the FeOOH dispersion, 20 mL ethanol, and 250 µL ammonium solution twice with 1-h intervals. The solution was magnetically stirred overnight. Later, FeOOH@SiO_2 was isolated and washed with ethanol once and water three times at 14,500 rpm for 10 min. Finally, to reduce the FeOOH@SiO_2, 25 mL TEG was heated to 280 °C under nitrogen, to which 250 µL concentrated FeOOH@SiO_2 was injected. The reaction was kept for 8 h under nitrogen protection. The final product was the Fe_3O_4@SiO_2 nanorods, which were washed with ethanol and water three times and dried under nitrogen for further use.

Synthesis of ZIP monomer carboxybetaine methacrylate (CBMA). 2-Carboxy-N,N-dimethyl-N(2′-(methacryloyloxy)ethyl)ethanaminium (CBMA) was synthesized according to the reported work. [1] In short, 0.76 mL (12 mmol) β-propiolactone dissolved in 10 mL dried acetone was added dropwise to 50 mL dried acetone containing 1.7 mL (10 mmol) DMAEM at 15 °C under stirring and incubated for 6 hour under nitrogen protection. The white precipitate was filtered off, washed with anhydrous acetone and ether, and dried under vacuum to receive CBMA as a white powder. ^{1}H NMR (D_2O, 400 MHz): δ 6.16 (s, 1H), 5.78 (s, 1H), 4.62 (t, 2H), 3.80 (t, 2H), 3.68 (t, 2H), 3.20 (s, 6H), 2.74 (t, 2H), 1.94 (s, 3H) (**Figure S11**).

Synthesis of Nanorods coated with various surface groups. Nanorod-COOH, Nanorod-NH_2 and Nanorod-PEG. The nanorods were firstly dispersed in ethanol and heated to 80 °C. After that, 200 μL of APTES was added quickly and reacted for around 5 hours to obtain the amine-modified nanorods. The nanorod-NH_2 was washed with ethanol four times and dried under vacuum.

For the nanorod-COOH, 4 g succinic anhydride was dissolved in 20 mL DMF, to which 4 mL APTES was added directly. The mixture was magnetically stirred overnight. The carboxyl-modified APTES could be used without any purification. Following, 10 mg nanorods were dispersed in DMF at a concentration of 1mg/mL under sonication. And then, 4 mL carboxyl-modified APTES in DMF was added to the nanorods dispersion and incubated at room temperature under the magnetic plate for 37 h. After that, the product nanorod-COOH was isolated by the external magnetic field and washed with DMF and ethanol three times.

For the nanorod-PEG, 100 μL 10 mg/mL nanorod-COOH was added to 1 mL MES (0.1 M, pH 5) solution containing (2 mg/mL EDC, 1mg/mL NHS). The mixture was incubated at room temperature for 2 hours. After that, the activated nanorod was isolated and washed with 1xPBS three times. And then, the activated magnetic nano-stir bar was redissolved in borate buffer (10 mM sodium borate, 150 mM NaCl, pH 8.5) containing 10 μg amine-modified mPEG and incubated at 4 °C overnight. Finally, the nanorod-PEG was obtained.

Preparation of the zwitterionic polymer layers on nanorod surface. Initially, nanorods coated with primary amines (nanorod-NH_2) were prepared (Supporting Information). At 0 °C, 3 mg of the nanorod-NH_2 was dispersed into 2 mL anhydrous N,N-dimethylformamide (DMF) and bubbled with nitrogen gas, followed by the addition of 0.35 mL triethylamine (TEA, 2.5 mol) and 0.175 mL α-bromoisobutyryl bromide (BIBB, 1.45 mmol). Then, the ice-cold solution was placed at room temperature (RT) and the mixture reacted for 12 hours under nitrogen protection. Next, the

nanorods were washed with DMF, iso-propanol and water sequentially, each for three times, and collected before the surface-initiated atomic transfer radical polymerization (SI-ATPR) was conducted, in which 3 mg of nanorods was dissolved in 1 mL of the oxygen-free solvent (water/iso-propanol 4:1) and the solution was purged with nitrogen for 15 min. The resulting nanorods were injected to the solution prepared by mixing 140 mg (1.05 mmol) carboxybetaine methacrylate (CBMA) (preparation procedure shown in Supporting Information), 30 mg (0.21 mmol) CuBr, and 68 mg (0.44 mmol) 2,2'-bipyridine (bpy) in 2 mL of the oxygen-free, water/iso-propanol 4:1 mix under N_2 protection. After two rounds of degassing, the mixture reacted at 25 °C for 16 h under N_2 protection. The reaction product was washed with isopropanol and water three times, before being dispersed in 4 mL 0.1 M aqueous sodium azide solution under N_2 protection. After 2-h reaction, which end-capped some of the polymer chains by the azide group to block further polymerization, the next round of polymerization was carried out with the same procedure but a shorter reaction time of 6 h, to further extend the Br-capped polymer chains.

Evaluation of nonspecific protein adsorption. Nonspecific adsorption of proteins on the nanorods with various coating materials was conducted by mixing 200 μg nanorods with undiluted serum at RT for 1 h. The nanorods were isolated and washed with 1× PBS three times. Then, 150 μL 1× PBS containing 5% SDS were added, and the mixture was incubated for 5 min at 25 °C. The supernatant was carefully removed upon magnetic separation and diluted with 350 μL 1× PBS. Then the protein amount in the supernatant was evaluated using the BCA assay according to the manufacturer's instructions (Micro BCA Protein Assay, Fisher Scientific).

Coupling PYR1 and HAB1 variants with the capture probes (CP). The CP modified-PYR1s were prepared via click reaction. Each modification was initiated by incubating 100 μL of 15 μM recombinant PYR1 with 1.5 μL of 50 mM NHS-$(PEG)_5$-DBCO at 4 °C overnight. The DBCO-modified PYR1 was purified via the 7KDa Zeba desalting column (ThermoFisher). The ratio between DBCO and protein was quantified by measuring the absorbance at 280 nm and 309 nm. The amine-modified CP was activated by NHS-$(PEG)_4$-azide at 4 °C overnight, and the azide-modified CP was purified by 7KDa Zeba desalting column. Finally, the DBCO modified PYR1 was mixed with the azide-modified capture probe in a ratio of 1 : 3 at 4 °C for overnight reaction.

Conjugation of nanorods with PYR1. Nanorod modification by the surface probes (SP) was through the carboxyl groups, which were either on the ZIP or on the carboxyl-decorated silica

surface. At first, 100 µL of 10 mg/mL the nanorod was added to 1 mL of 0.1 M MES (pH 5) containing 2 mg/mL EDC and 1 mg/mL NHS. The mixture was incubated at RT for 2 h; and then the activated nanorod was isolated, washed with 1× PBS three times, redissolved in 10 mM sodium borate at pH 8.5 containing 150 mM NaCl, and mixed with 20 µL of 100 µM the amine-modified SP. Upon overnight incubation at 4 °C, the remaining NHS ester on the nanorods was deactivated by 10 mM sodium carbonate (pH 10). At last, the capture probe (CP)-PYR1 was mixed with the SP-modified nanorod at RT for 20 min to obtain the PYR1-conjugated nanorods for drug detection.

Protein production. MBP-tagged proteins were expressed in BL21(DE3)pLysS host cells as previously reported.[i,ii] Sumo-tagged proteins were expressed in BL21(DE3)pLysS host cells induced with 1 mM isopropyl β-D-1 thiogalactopyranoside (IPTG) (OD_{600} = 0.8) for 12 hours at 18 °C. To obtain the 6×-His-Sumo PYR1 variant fusion constructs, PYR1 coding sequences (aa 1-181) and the full pET28 SUMO backbone were PCR amplified (primers used can be found in Supporting Information), resulting in adjacent DNA fragments with complementary ends. The PCR fragments were then assembled using the NEBuilder® HiFi DNA Assembly Cloning Kit (New England Biolabs), and the plasmids obtained were confirmed by Sanger sequencing and used for preparation of the recombinant proteins. Two versions of recombinant HAB1 were used in this work: the HAB1 N-terminal deletion mutant (ΔN-HAB1, lacking the first 178 N-terminal amino acids) which is catalytically active; and ΔN-HAB1^{T+}, a catalytically inactive variant relative to ΔN-HAB1 and engineered for improved expression and thermos-stability. ΔN-HAB1 is a 6×-His fusion protein produced as described in previous reported work;[i, iii] and ΔN-HAB1^{T+} is a MBP fusion protein produced as described in Steiner *et al*.[ii] They were referred as His- ΔN-HAB1 and MBP-ΔN-HAB1^{T+}.

Related references:

i. Vaidya, A. S.; Helander, J. D. M.; Peterson, F. C.; Elzinga, D.; Dejonghe, W.; Kaundal, A.; Park, S. Y.; Xing, Z. N.; Mega, R.; Takeuchi, J.; Khanderahoo, B.; Bishay, S.; Volkman, B. F.; Todoroki, Y.; Okamoto, M.; Cutler, S. R. Science 2019, 366, eaaw8848.

ii. Steiner, P. J.; Bedewitz, M. A.; Medina-Cucurella, A. V.; Cutler, S. R.; Whitehead, T. A. Aiche J 2020, 66, e16767.

iii. Vaidya, A. S.; Peterson, F. C.; Yarmolinsky, D.; Merilo, E.; Verstraeten, I.; Park, S.-Y.; Elzinga, D.; Kaundal, A.; Helander, J.; Lozano-Juste, J.; Otani, M.; Wu, K.; Jensen, D. R.; Kollist, H.; Volkman, B. F.; Cutler, S. R. ACS Chemical Biology 2017, 12, 2842-2848.

Modification of His-ΔN-HAB1 with biotin. To get biotin-modified His-ΔN-HAB1 (without phosphatase activity), the His-ΔN-HAB1 was mixed with NHS-biotin in a ratio of 1:10, and the mixture was incubated at 4 C overnight. The unreacted biotin molecules were removed via the 7KDa Zeba desalting column. The purified biotin-HAB1 was stored in the 10% vol/vol glycerol, 50 mM HEPES of pH 8.0, 200 mM KCl, 10 mM $MnCl_2$, 1 mM DTT, and 1 mM TCEP at -80 °C.

2. Primers used in SUMO protein expression and sequences of fusion proteins MBP and SUMO.

Name	**Sequence**
Vector primers used for construction of pET-SUMO	pET-SUMO Forward (Fw): AAGCTTCTCGAGCACCACCACC pET-SUMO Reverse (Rv) primer: ACCACCAATCTGTTCTCTGTGAGC
Insert primers used for construction of SUMO-PYR1 fusion	PYR1-Fw-SUMO: GCTCACAGAGAACAGATTGGTGGTATGCCTTCGGAGTTAACACCAG PYR1-Rv-SUMO: GGTGGTGGTGCTCGAGAAGCTTAGTTACGAGCCATAGCTTCAGCAAC
Protein sequence for MBP tag	SSGMKIEEGKLVIWINGDKGYNGLAEVGKKFEKDTGIKVTVEHPDKLEEKFPQVAATGDGPDIIFWAHDRFGGYAQSGLLAEITPDKAFQDKLYPFTWDAVRYNGKLIAYPIAVEALSLIYNKDLLPNPPKTWEEIPALDKELKAKGKSALMFNLQEPYFTWPLIAADGGYAFKYENGKYDIKDVGVDNAGAKAGLTFLVDLIKNKHMNADTDYSIAEAAFNKGETAMTINGPWAWSNIDTSKVNYGVTVLPTFKGQPSKPFVGVLSAGINAASPNKELAKEFLENYLLTDEGLEAVNKDKPLGAVALKSYEEELVKDPRIAATMENAQKGEIMPNIPQMSAFWYAVRTAVINAASGRQTVDEALKDAQT
Protein sequence for SUMO tag	MGHHHHHHGSLQDSEVNQEAKPEVKPEVKPETHINLKVSDGSSEIFFKIKKTTPLRRLMEAFAKRQGKEMDSLTFLYDGIEIQADQTPEDLDMEDNDIIEAHREQIGG

3. Nanorod characterization

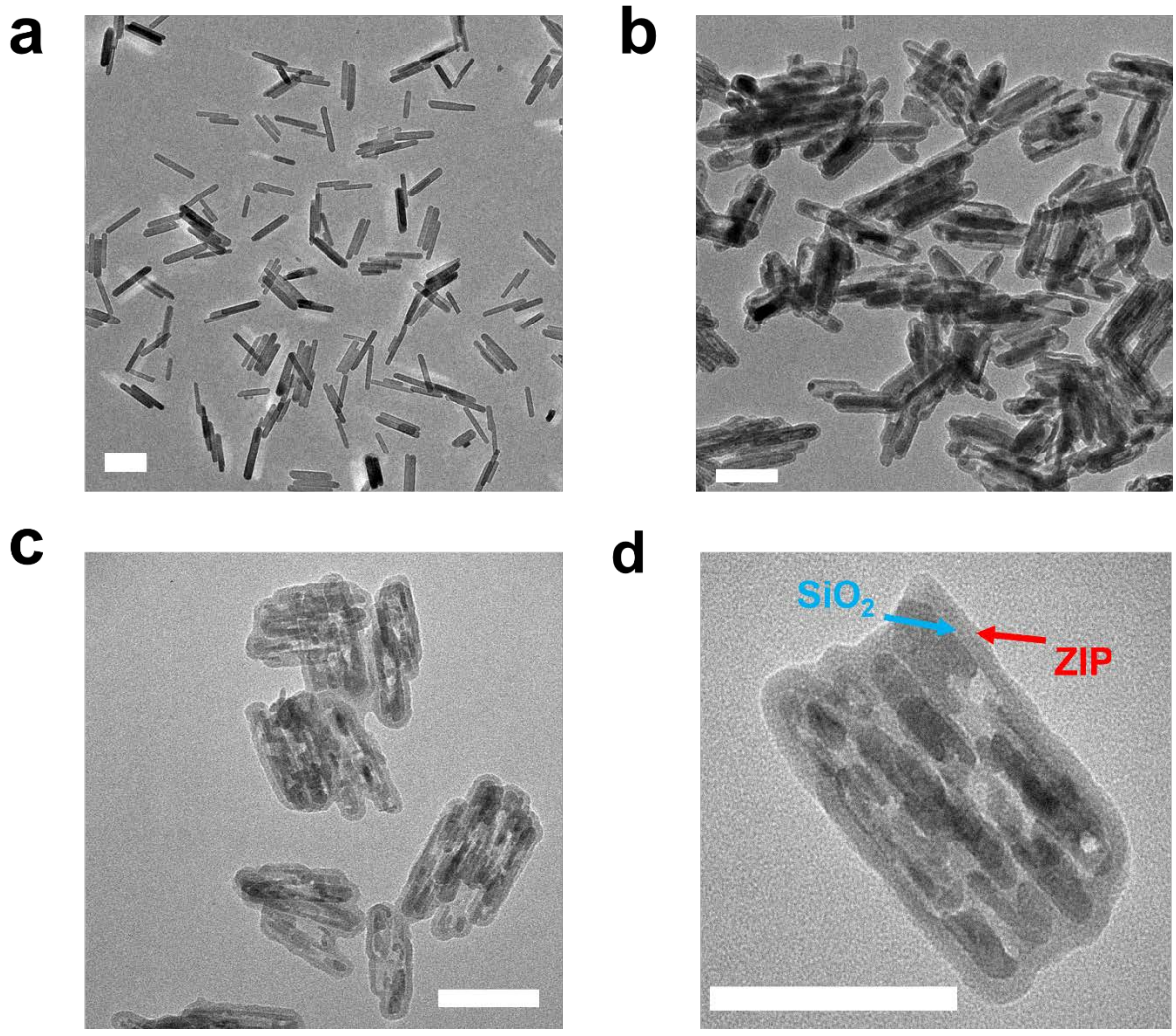

Figure *S*-1. TEM image of nanorods: FeOOH (a), Fe_3O_4@SiO_2 nanorods (b), nanorod-ZIP-DL (c-d). The scale bar is 100 nm

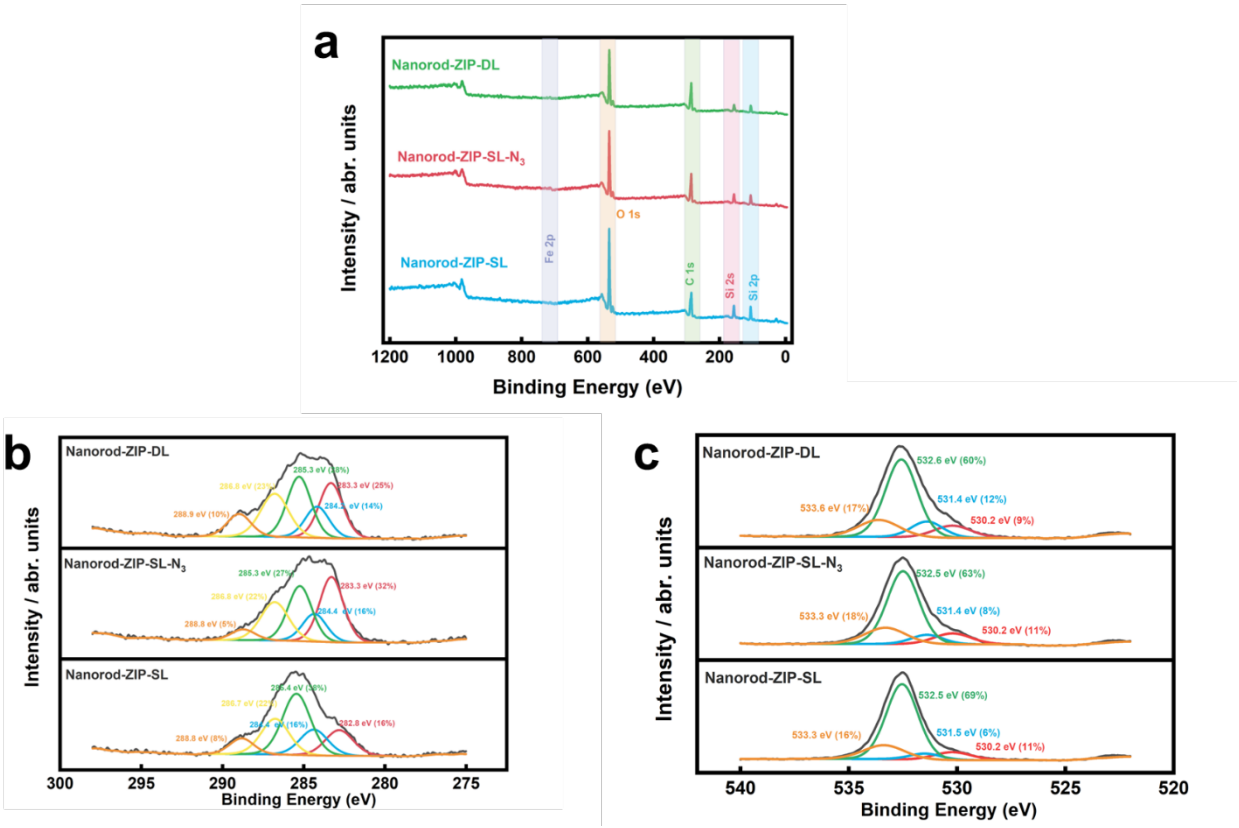

Figure *S*-2. a, Survey XPS data of nanorod-ZIP-SL, nanorod-ZIP-SL-N_3, and nanorod-ZIP-DL. **b,** C1s deconvolution XPS spectra of nanorod-ZIP-SL, nanorod-ZIP-SL-N3, and nanorod-ZIP-DL, where peaks at 284.4 Ev, 284.5 eV, 286.7 eV, and 288.8 eV belong to C-C, C-N, C-O and C=O respectively; **c,** O1s deconvolution XPS spectra of nanorod-ZIP-SL, nanorod-ZIP-SL-N3, and nanorod-ZIP-DL, where peaks at 532.2 eV, 531.4 eV, 532.5 eV, and 533.5 eV belong to the Fe-O, C=O, SiO_2, and C-O respectively.

4. Difference Surface Modification Comparison

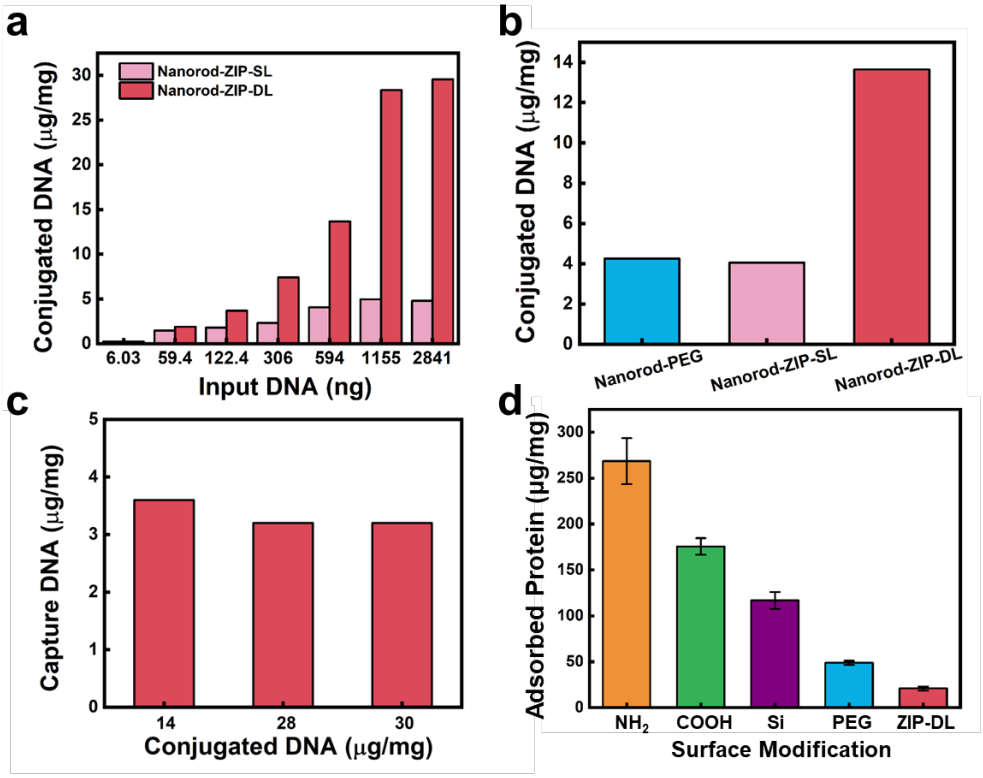

Figure *S*-3. **a,** Conjugation efficiency comparison between nanorod-ZIP-SL and nanorod-ZIP-DL. 20 μg nanorod-ZIP was used to conjugate with different DNA input via EDC/NHS coupling. The unreacted DNA left in the supernatant was quantified via Qubit. **b,** Conjugation efficiency comparison between different surface modifications: PEG, ZIP-SL, and ZIP-DL. 20 μg nanorod-ZIP was used to conjugate with 594 ng DNA input. **c,** Comparison of the amount of CP immobilized on 1 mg of the nanorod with different immobilized DNA amount. The input complementary DNA strand was 50 pM (210 ng). **d,** non-specific adsorption comparison between different surface properties (-NH_2, -COOH, Si, PEG, and ZIP) in human serum albumin, of which 200 μg nanorod with different surface properties was incubated with 200 μL HSA solution (45 mg/mL) and the adsorbed protein was quantified via the MicroBCA kit.

5. PYR1 and HAB1 Conjugation

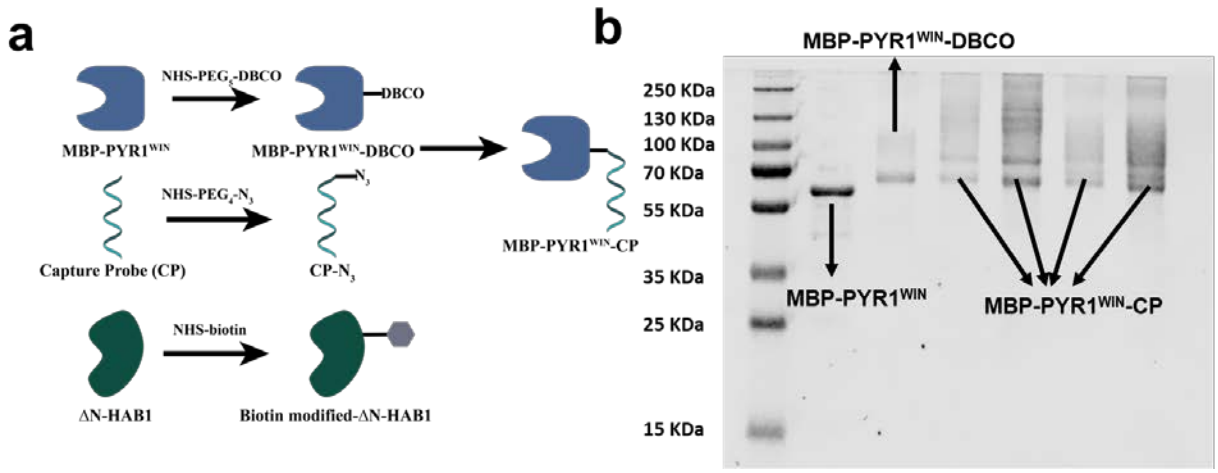

Figure *S*-4. a, the conjugation scheme; **b,** the PAGE gel to prove the successful conjugation DNA to the MBP-PYR1^{WIN} and the ratio between DNA and MBP-PYR1^{WIN} was 3-5.

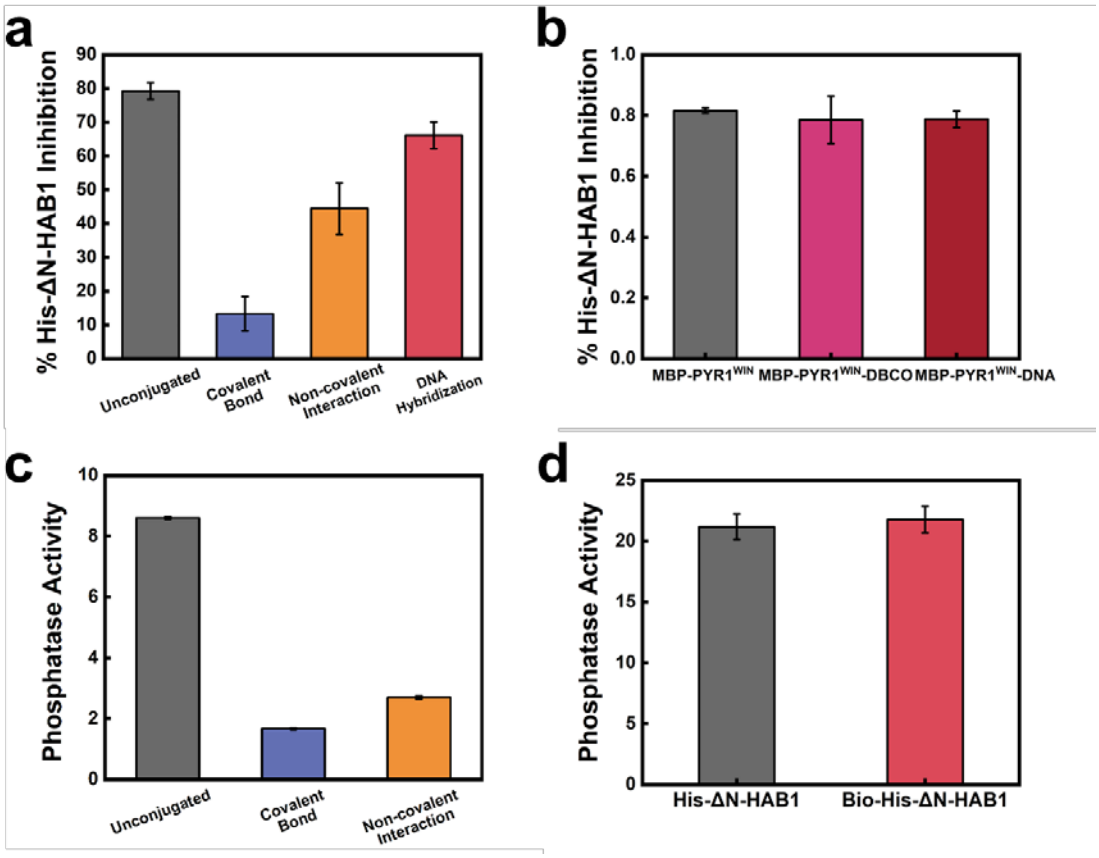

Figure *S*-5. a, conjugate method effect on the MBP-PYR1^{WIN} binding performance; **b,** small molecule modification effect on the PYR1 binding performance; **c,** conjugate method effect on the His-ΔN-HAB1 phosphatase activity; **d,** biotinylation effection on the His-ΔN-HAB1 phosphatase. The binding performance and phosphatase activity were evaluated via the ligand-dependent inhibition of His-ΔN-HAB1 phosphatase activity assay. The concentration of His-ΔN-HAB1, MBP-PYR1^{WIN}, WIN, and 4-methylumbelliferyl phosphate were 50 nM, 50 nM, 10 μM and 10 mM.

6. Cannabinoid detection performance

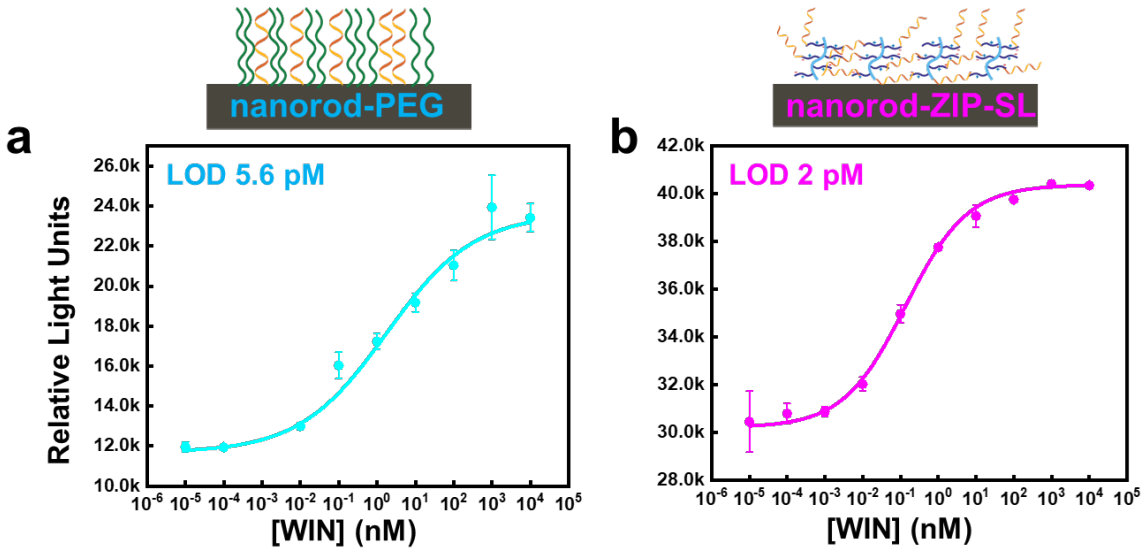

Figure *S*-6.WIN detection in saline assisted by the nanorods carrying different surface modifications. a) PEG modification. b) Single layer zwitterionic polymer modification. The blank was 4017±997, and 3341±36 for **nanorod-PEG** and **nanorod-ZIP-SL**, separately. Each data point represents the mean of three replicates, with the error bar representing the standard deviation; and the LOD was calculated via the 3σ method.

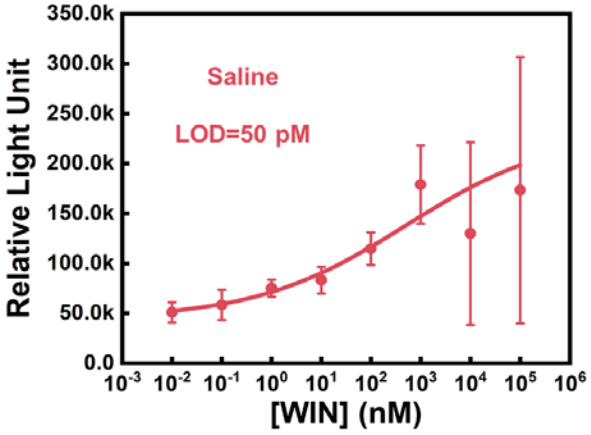

Figure *S*-7. WIN detection performance by conventional ELISA assay with chemiluminescence in saline. Each dot represents the mean of three replicates, and the LOD was calculated via the 3σ. The blank was 44007.67±4723.88. The concentration of MBP-PYR1^{WIN}, MBP-ΔN-HAB1^{T+} was 1 μM.

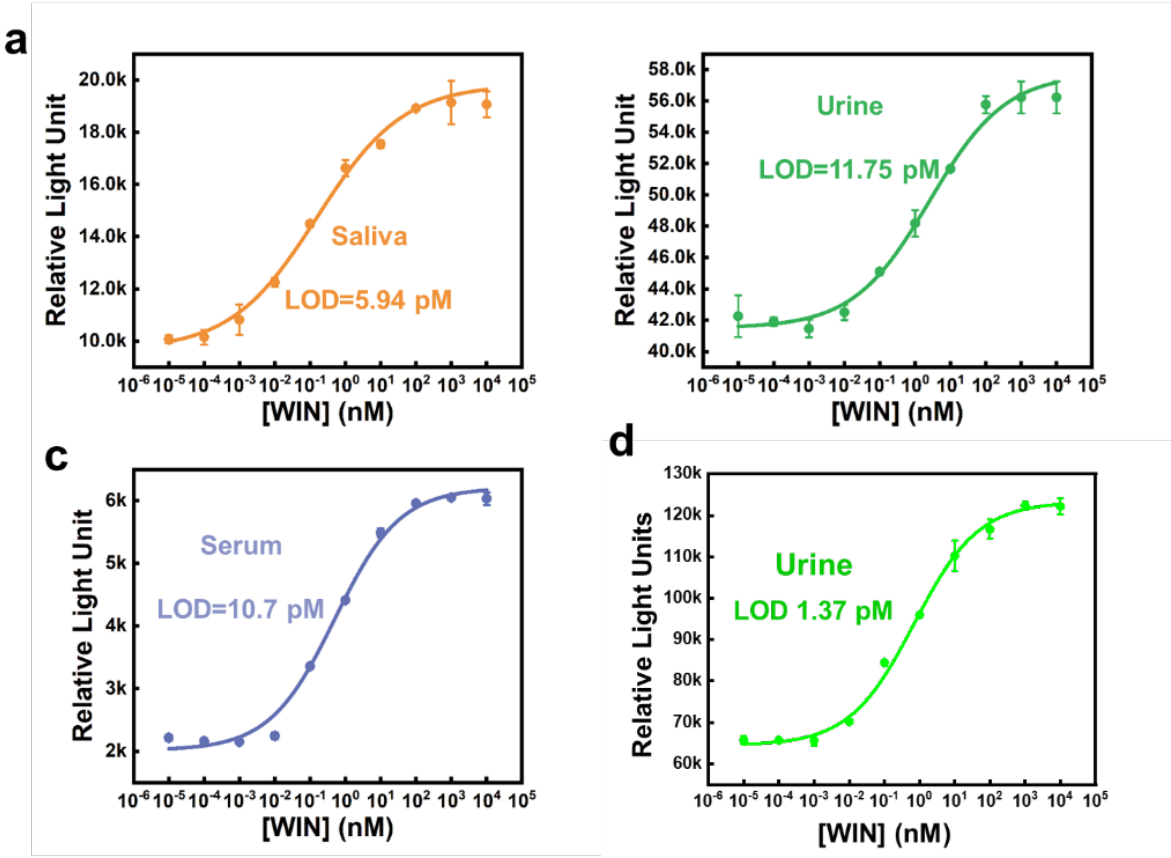

Figure *S*-8. WIN detection performance assisted by the **nanorod-PEG** with nanorod-assisted ELISA-like assay in pure saliva (**a**), urine (**b**), and serum (**c**). **d**) WIN detection performance assisted by the **nanorod-ZIP-DL** with nanorod-assisted ELISA-like assay in pure urine. Each dot represents the mean of three replicates, and the LOD was calculated via the 3σ. The blank in saliva, urine and serum of **nanorod-PEG** was 10022±581, 36842±481, 2041±36, separately. And the blank in urine of **nanorod-ZIP-DL** was 57787±524.

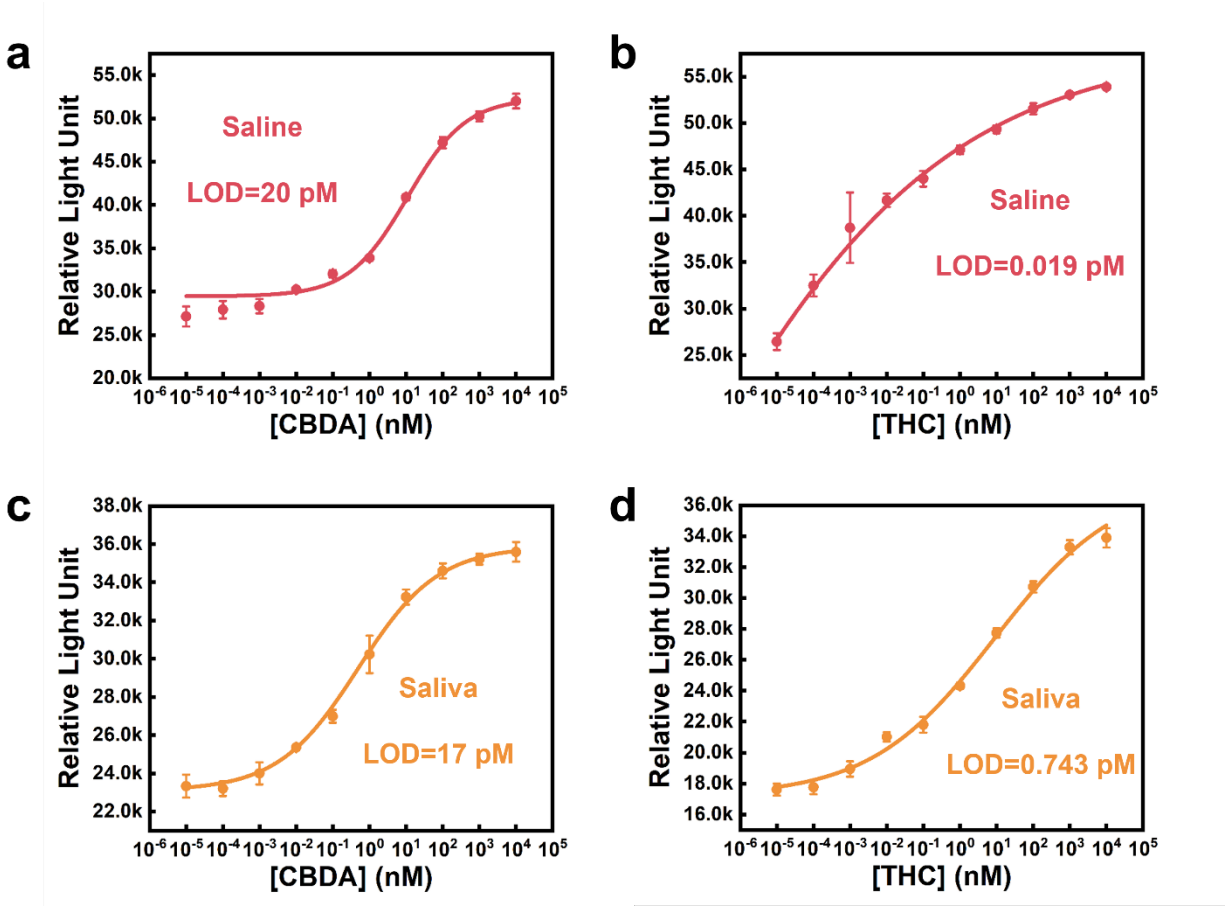

Figure *S*-9. CBDA (**a, c**) and THC (**b, d**) detection performance assisted by the nanorod-ZIP-DL with nanorod-assisted ELISA-like assay in pure saline and saliva. Each dot represents the mean of three replicates, and the LOD was calculated via the 3σ. The blank for CBDA in saline and saliva was 21218±831, 17284±2740 separately. The blank for THC in saline and saliva was 22467±1909, 14012±533 separately.

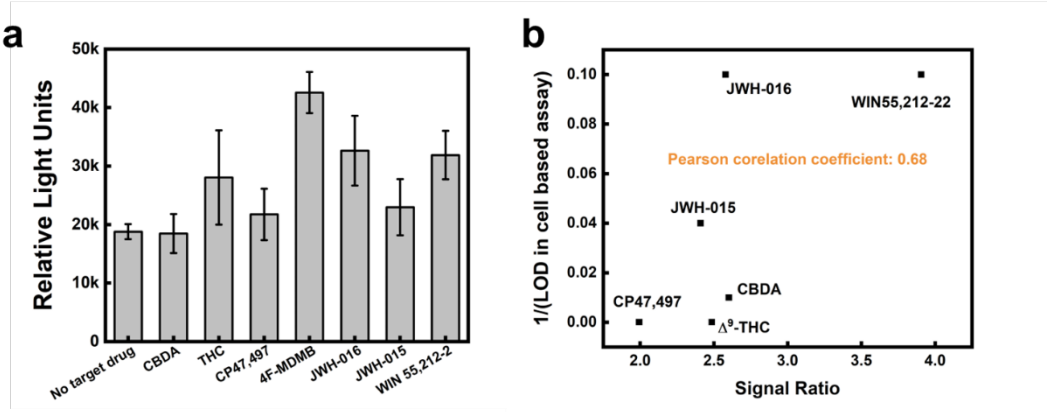

Figure *S*-10. a, 4F-MDMB detection specificity towards other cannabinoids with nanorod-assisted ELISA-like assay (THC, CBDA, JWH-015, JWH-016, CP47, 497, WIN 55, 212-2). The concentration of each drug was 1 μM, and the receptor used here was His-PYR1^{4F}. The signals were generated by using the nanorod-ZIP-DL conjugated to the PYR1 variant specific for the target drug. Each drug in the mixture was at 1 μM. The results were the average value and the standard deviation (error bar) from three replicates. **b,** the correlation between signal ratio in nanorod-assisted ELISA- like assay and 1/LOD in the cell-based assay.

7. ^{1}H NMR

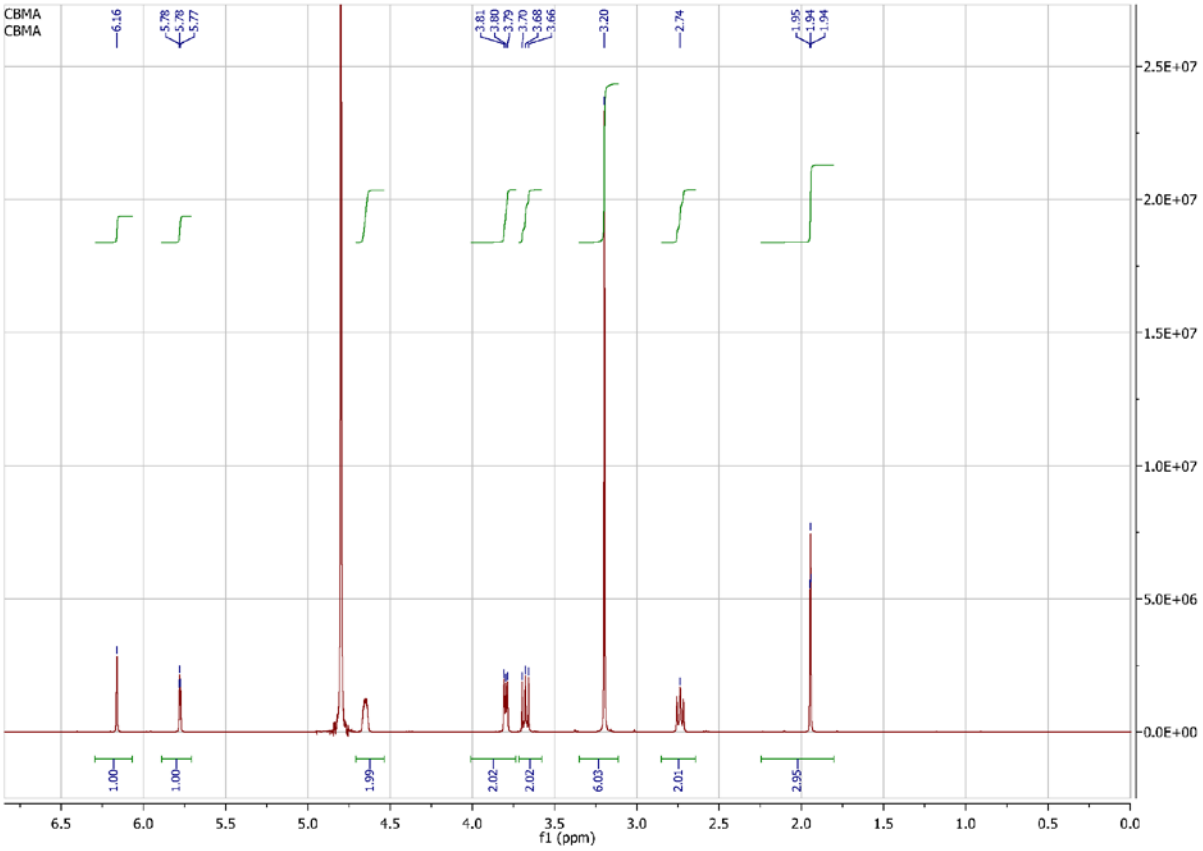

Figure *S*-11. ^{1}H NMR of CBDA

8. Performance comparison with techniques reported in literature.

Target	Signaling Approach	Limited of Detection	Linear Range	Response Time	Biofluids used	Antifouling Method
Δ^9-tetrahydro-cannabinol (THC)[2]	Fluorescence	0.01 ng/mL	0.01-10 ng/mL	5 min	Oral fluids	Not applied
Cocaine[3]	Fluorescence	209 pM	0.5-20 nM	40 min	Pretreated and diluted serum	Not applied
JWH-018[4]	Colorimetric	0.68 μg/mL	3-25 μg/mL	> 5 min	Not tested	Not applicable
THC/CBD[5]	Electro-chemical	3.27 μg/mL for THC and 2.85 μg/mL for CBD	10–500 μg/mL	20 min	Not tested	Not applicable
THC[6]	SERS	1 pM	1 pM-1 mM	15 min	Plasma and saliva	Not applied
methadone, METH, amphetamine, THC[7]	Chemi-luminescence	1.6 pg mL^{-1} for methadone; 142 pg mL^{-1} for METH; 35 pg mL^{-1} for amphetamine; 20 pg mL^{-1} for THC	methadone: 0.0016–1 ng mL^{-1}; METH: 0.016–25 ng mL^{-1}; amphetamine: 0.005–10 ng mL^{-1}; THC: 0.02–1000 ng mL^{-1}	16 min	Sweat	Surface passivation by 1% BSA
THC[8]	Colorimetric	Not mentioned	1–10 μg/mL	15 min	Not tested	Surface passivation by BSA

9. References

1. Huang, C. J.; Li, Y. T.; Jiang, S. Y., Zwitterionic Polymer-Based Platform with Two-Layer Architecture for Ultra Low Fouling and High Protein Loading. *Anal Chem* **2012,** *84* (7), 3440-3445.
2. Plouffe, B. D.; Murthy, S. K., Fluorescence-based lateral flow assays for rapid oral fluid roadside detection of cannabis use. *Electrophoresis* **2017,** *38* (3-4), 501-506.
3. Emrani, A. S.; Danesh, N. M.; Ramezani, M.; Taghdisi, S. M.; Abnous, K., A novel fluorescent aptasensor based on hairpin structure of complementary strand of aptamer and nanoparticles as a signal amplification approach for ultrasensitive detection of cocaine. *Biosens Bioelectron* **2016,** *79*, 288-293.
4. Durmus, H.; Durmazel, S.; Uzer, A.; Gokdere, B.; Ercag, E.; Apak, R., Colorimetric Determination of (Aminoalkyl)indole-containing Synthetic Cannabimimetics. *Anal Sci* **2018,** *34* (12), 1419-1425.

5. Pholsiri, T.; Lomae, A.; Pungjunun, K.; Vimolmangkang, S.; Siangproh, W.; Chailapakul, O., A chromatographic paper-based electrochemical device to determine Delta(theta)-tetrahydrocannabinol and cannabidiol in cannabis oil. *Sensor Actuat B-Chem* **2022,** *355*.
6. Sivashanmugan, K.; Squire, K.; Tan, A. L.; Zhao, Y.; Kraai, J. A.; Rorrer, G. L.; Wang, A. X., Trace Detection of Tetrahydrocannabinol in Body Fluid via Surface-Enhanced Raman Scattering and Principal Component Analysis. *Acs Sensors* **2019,** *4* (4), 1109-1117.
7. Xue, W.; Tan, X. T.; Oo, M. K. K.; Kulkarni, G.; Ilgen, M. A. A.; Fan, X. D., Rapid and sensitive detection of drugs of abuse in sweat by multiplexed capillary based immuno-biosensors. *Analyst* **2020,** *145* (4), 1346-1354.
8. Solin, K.; Vuoriluoto, M.; Khakalo, A.; Tammelin, T., Cannabis detection with solid sensors and paper-based immunoassays by conjugating antibodies to nanocellulose. *Carbohyd Polym* **2023,** *304*.